R & M No. 3839

R & M No. 3839

PROCUREMENT EXECUTIVE, MINISTRY OF DEFENCE

Aeronautical Research Council
Reports and Memoranda

THE BOUNDARY LAYER DEVELOPMENT DOWNSTREAM OF A SHOCK INTERACTION AT AN EXPANSION CORNER

by

Y.T. Chew and L.C. Squire

Cambridge University Engineering Department

London: Her Majesty's Stationery Office
1979
PRICE £9 NET

UDC 532.526 : 533.6.048.6 : 533.6.011.72 : 532.556 : 533.6.071

THE BOUNDARY LAYER DEVELOPMENT DOWNSTREAM OF A SHOCK INTERACTION AT AN EXPANSION CORNER

By Y.T. Chew* and L.C. Squire
Cambridge University Engineering Department

Reports and Memoranda No.3839**
August 1978

SUMMARY

Boundary layer developments have been measured for the flow downstream of an expansion corner when the boundary layer is disturbed by a shock wave striking the surface near the corner. It is found that most velocity profiles quickly relax to a near-equilibrium state in about 8 to 16 boundary-layer thicknesses with the actual distance depending on the shock strength. However, this equilibrium state is not the same as that in a flat-plate boundary layer at the same Mach number and Reynolds number. In spite of this, the velocity profiles downstream of the interaction collapse onto the low-speed law of the wall when plotted in terms of Van Driest's transformed velocity coordinates.

The boundary layer developments are in fair agreement with the predictions from an eddy-viscosity model when the incident shock is weak. For stronger shocks the calculated profiles from the eddy-viscosity model and from Bradshaw's turbulent energy method are similar, but both fail to predict the measured boundary layer development. However, the agreement was much improved if the calculation was started from the first measured profile after the shock interaction, and the prediction from the eddy-viscosity model was further improved if an exponential lag equation was used to account for the transport properties of the turbulence.

---

* Present address - Department of Mechanical Engineering,
University of Singapore,
Kent Ridge Campus,
Singapore 5

** Replaces ARC 37 863

LIST OF CONTENTS

1. INTRODUCTION

In spite of the large number of investigations of turbulent boundary layers in compressible flow there is still a lack of data on the boundary-layer development downstream of a strong disturbance, such as a shock-wave/boundary-layer interaction. Furthermore the investigations which do exist show that most calculation methods are weakest in the relaxing flow downstream of a disturbance. There is thus a need for more experimental results in flows of this type, both to provide data on the relaxation process and to provide test cases for prediction methods.

This paper describes seven boundary layer developments measured during the course of an investigation of the interaction of an oblique shock wave with the boundary layer passing over an expansion corner. In addition to studying the case when the shock wave struck the boundary layer exactly at the corner, cases when the shock struck upstream and downstream of the corner were also studied (Fig. 1). As a result the boundary layer was subjected to a variety of pressure distributions, such as a sudden rise in pressure followed by a rapid fall when the interaction was upstream of the corner and the reverse situation when the interaction was downstream. Downstream of this 'square-wave' type of pressure distribution the pressure was approximately constant for about 20 boundary-layer thicknesses (Fig. 2) and it was possible to study the development of the boundary layer in this constant pressure region.

The present paper presents the results of these boundary-layer surveys and compares the results with predictions from two calculation methods. In addition the results of various modifications to a calculation method based on eddy viscosity are described.

2. DETAILS OF EXPERIMENTS

2.1 Tunnel

The tests were made in an intermittent blowdown tunnel in the Cambridge University Engineering Department. A sketch of the working section together with the main dimensions are given in Fig. 3 and photographs of the test arrangements are shown in Fig. 4. Full details of the tunnel are given by Chew[1,2] and here it is only necessary to note that the angle of the shock generator could be varied to give shocks of different strengths and that the test surface could be moved in the longitudinal direction so that the shock impingement point varied relative to the corner.

2.2 Pitot pressure profiles

Fig. 4 shows the arrangements used to measure the boundary-layer developments. Basically the system is similar to that designed by Jeromin[3] and subsequently improved and used by Squire[4], Dunbar[5], Thomas[6] and Marriott[7] although in the present tests the data was recorded by a data-logger rather than on an x-y recorder. In this system the pitot pressure through the layer is measured by a pitot tube mounted on a hand-driven traverse gear. The tube was made from 1 mm o.d. hypodermic tube which was flattened and filed to give a tip with a rectangular section of height 0.184 mm and a width of 1.550 mm. The tip was not exactly symmetrical and it is estimated that the effective centre of the probe is 0.09 mm from the lower surface.

The position of the probe was measured by an electrical signal from a sliding potentiometer and it is estimated that the error of the calibration of the signal is less than 0.05 mm. In addition to the accuracy of the calibration it is necessary to fix the absolute position of the probe relative to the wall. This absolute position was determined when the probe just left the surface by the breaking of a circuit containing a light-emitting diode as indicator. This gave a reference point on the calibration curve which could be determined to $\pm$ 0.03 mm.

No displacement corrections were applied to the probe position since the average value of the ratio of probe height to boundary-layer thickness was 0.025. Since Allen[8] has shown that displacement effects are negligible if this ratio is less than 0.02 it was considered that the displacement correction was likely to be small compared with the errors in the position measurement.

2.3 Static pressure profiles

The static pressure profile across the layer was obtained by replacing the pitot tube by a conical static probe. This probe had a conical nose with a total angle of 5^{o} soldered into the end of a 1 mm o.d. hypodermic tube. Two static holes of 0.4 mm diameter were drilled into the top and bottom of the tube 14 mm downstream of the joint with the conical tip. It was found that the static pressure varied by less than 1% across the boundary layer for all profiles upstream of the shock and for all profiles more than 50 mm downstream of the interaction. Closer to the interaction the variation rose to a maximum of 4%. However, in many cases where this maximum variation was found the tip of the probe intersected the shock so it is not clear that the variation is genuine.

2.4 Temperature measurements

Originally it had been intended to measure the static temperature across the boundary layer with a conical equilibrium probe as used by Jeromin[3]. However,

it was found that both the tunnel stagnation temperature and the wall temperature varied during the 60 second run of the tunnel*. In particular at the beginning of the run the recovery temperature (based on a recovery factor of 0.89) was up to 14° below the corresponding wall temperature and during the run the recovery temperature rose by up to 6°C. At the same time the wall temperature fell slowly so that the difference between wall and recovery temperature narrowed and settled to a value of about 6°C. Allowing for lag effects in the probe this raised considerable doubts as to the value of direct measurements of static temperature made in a separate run from the pitot traverse. It was therefore decided to record the instantaneous values of stagnation and wall temperature at each reading of the pitot tube. The static temperature was then deduced from the Crocco relation -

$$T = T_w + (T_r - T_w)(u/U) + (T_1 - T_r)(u/U)^2 \qquad (1)$$

where T_r is the recovery temperature based on a recovery factor of 0.89.

2.5 Skin-friction measurements

Skin-friction was measured by a Preston tube of 0.419 mm o.d. with an inner to outer diameter ratio of 0.5. To use this tube the traverse gear was wound towards the surface so that the tip of the probe lay on the surface and was held in position by tension created by the bending of the support tube. As the tunnel started the tip of the probe moved sideways and then settled to a steady position. If the probe mounting was correct this steady position was at zero yaw angle; the test was repeated if the yaw angle was greater than 5°. A number of tests were made with the probe not quite parallel to the surface and the results showed that the measured readings should be accurate to better than ½%.

3. REDUCTION AND ACCURACY OF RESULTS

3.1 Velocity profiles

As mentioned in section 2.3 the static pressure was almost constant across the layer and so it was decided to ignore the measured variations in the analysis. Furthermore, considerations of possible losses through the interaction region showed that the static pressure measured by the wall pressure holes was more accurate than the static pressure deduced from the pitot-tube reading in the

---

* The changes in temperature do not appear to have been so large in the work reported in Refs. 3 to 7. In part this may be due to the fact that the present tests were made in a different test section to that used in earlier work. However, the main reason is probably that the data logger used in the present study is more accurate than the x-y recorder system used in the past.

free stream and the tunnel stagnation pressure. Thus the local Mach number at a point in the boundary layer was found from the ratio of the wall static pressure directly below the point and the local reading of the pitot tube.

The velocity profile was then obtained from the Mach number profile by assuming that the local static temperature was given by the Crocco relation (eqn. (1)) based on the instantaneous values of wall and stagnation temperature. The accuracy of this assumption was checked by recalculating some profiles with the assumption that the stagnation temperature was constant across the layer. It was found that the values of θ, δ^* and H calculated under the assumption of constant stagnation temperature differ from those using the Crocco relation by, at most, -3.0% (-0.017 mm), 1% (0.019 mm) and 3.8% (0.14) respectively. As the results of Winter and Gaudet[9] indicate that the calculated values of these parameters using measured temperatures lie between the values obtained with the above two assumptions, the magnitude of the errors suggest that the use of the Crocco relation should be satisfactory. A further check on the accuracy was made by recalculating some results using the Crocco relation based on run-mean temperatures rather than instantaneous values. In general the differences between corresponding values of θ, δ^* and H were about a quarter of the differences quoted above.

In order to obtain the integral parameters the experimental profiles were first interpolated to a fixed y-grid by using Aitken-Lagrange interpolation. In this grid 50 data points were set up over a distance of 10 mm from the wall such that the interval in y increased in a geometric progression with a ratio of 1.07 between adjacent intervals (this grid system was used since it was also required for the derivation of shear-stress profiles as described in section 3.3 below). The integral parameters were then found by trapezoidal integration. In addition to the usual integral parameters various transformed and kinematic parameters were found. The definitions of these parameters are given in Appendix A and all the values are tabulated in Table I.

Since the tunnel run was limited to about 60 seconds and the data logger required at least 2 seconds to record each set of data it was only possible to measure 20 - 25 points through the boundary layer in each run. In order to obtain more data two traverses were made at each position. Each run was reduced to a velocity profile and each individual profile was integrated for the integral parameters. Thus two values of parameters were obtained for each station as tabulated in Table I. As will be seen the corresponding values of the integral parameters at each station are in excellent agreement. For example, of the 49 pairs of values of θ, 26 pairs agree to within 0.006 mm (in a typical value of 0.5 mm) and only two of the pairs differ by more than 0.015 mm.

3.2 Skin friction

The size of the Preston tube was chosen according to the design criteria of Hopkins and Keener[10] and the skin-friction coefficients were first found using their calibration. Later the data was re-analysed using Allen's[11] calibration and these results are used in this paper. A comparison of the values of c_f from the two calibrations showed that the values obtained from the calibration of Hopkins and Keener were generally about 3% lower than those obtained from the calibration of Allen.*

3.3 Shear-stress profiles

Since the maximum length of tunnel run was too short to calibrate, and use, hot wires the turbulent shear stress across the layer was calculated from the mean velocity profiles. Basically the shear stress at $y = y_1$ is given by

$$\tau = \tau_w + \int_o^{y_1} \frac{\partial}{\partial x}(\rho u^2)dy - u(y_1)\int_o^{y_1} \frac{\partial}{\partial x}(\rho u)dy + y_1 \frac{dp}{dx} \qquad (2)$$

However, since this equation involves a number of differentiations of experimental data before integration it is likely to produce large variations in τ. Thus, following Marriott[7], the equation was rewritten so that one differentiation was carried out at the end, i.e.

$$\tau = \tau_w + \frac{\partial}{\partial x}\{I_1 - u(y_1)I_2 + I_3\}_{y=y_1} + y_1 \frac{dp}{dx} \qquad (3)$$

where

$$I_1 = \int_o^{y_1} (\rho u^2)dy$$

$$I_2 = \int_o^{y_1} (\rho u)dy$$

$$I_3 = \int_{u_o(y_1)}^{u(y_1)} I_2(u)du$$

and $u_o(y_1)$ is the value of $u(y_1)$ at the initial station. As explained above the experimental profiles were first interpolated to a fixed y-grid and the integrations were made by the trapezoidal rule. The final differentiation was performed by fitting a least-square polynomial to the data at fixed y. The skin-friction obtained from the Preston tube was used to find τ_w and the pressure gradient in eqn. (3) was chosen to force the shear stress to zero at

---

* In a recent paper Allen has introduced a new calibration curve but in the present tests the resultant changes in c_f are at most 2%.

the outer edge of the boundary layer. Thus the measured pressure gradient was not used.

Although Marriott claimed that eqn. (3) was more satisfactory than eqn. (2) it should be pointed out that the sum of the integrals in eqn. (3) is much smaller than the individual terms and that the difference between τ and τ_w is small compared with the two x-derivative terms. Thus the final shear stress is the difference of a number of large quantities. Also the final results are strongly dependent on the degree of the polynomial chosen for the least-square fit.

3.4 Two-dimensionality

So far the discussion of accuracy has centred on the measurement techniques and on repeatability. In addition it is necessary to consider the two-dimensionality of the test arrangement. From the pressure distributions (Fig. 2) it is clear that there is a difference in the shape of the pressure distribution along the centreline of the test plate and that along lines 19 mm away from the centreline. This difference is largest for the weakest shock. Chew[1] has shown that these differences are due to the influence of the side-wall boundary layers which tend to curve the incident shock, so producing a more forward impingement point off the centreline. In order to quantify the effects of this three-dimensional flow the two-dimensional momentum integral equation was integrated numerically along the flow using measured values of c_f, U, M and H. For the upstream flow the integration started from the first measured value of Θ. Similarly for flows downstream of the interaction the integration started from the measured value of Θ at the first downstream station. The calculated values of Θ are compared with the measured values in Fig. 5a. As will be seen the agreement between the measured and calculated values of Θ is satisfactory, although the discrepancies are as high as 6% for the flow just downstream of the 6° shock at the corner (Fig. 5a).

4. RANGE OF TESTS

All the profiles were obtained using a nozzle for $M = 2.5$ at a stagnation pressure of $0.515\ MN/m^2$ and a free-stream Reynolds number of 5×10^7 per metre. Boundary-layer developments were measured upstream (Case a) and downstream (Case b) of the expansion corner without an incident shock and for five flows downstream of the corner with a shock interaction. These five cases consisted of the interactions resulting from shocks with deflection angles of 4°, 6° and 8° striking the surface exactly at the expansion corner (Cases c, d and e respectively) and the interactions with the 6° shock striking the surface 20 mm upstream (Case f) and 20 mm downstream (Case g) of the corner. Seven boundary-

layer profiles were measured for each configuration. The schlieren photographs corresponding to the test flows are shown in Fig. 1 and the corresponding pressure distributions in Fig. 2.

5. DISCUSSION OF BOUNDARY-LAYER DEVELOPMENTS

The measured boundary-layer developments for the seven configurations tested are presented and discussed in this section. They are first studied in terms of the velocity and shear-stress profiles, together with the skin-friction and the various integral parameter distributions. The velocity profiles are then presented in the Van Driest's transformed velocity form so that they can be examined in relation to the inner and outer laws of the boundary layer.

5.1 Velocity profiles

All the results are plotted together as u/U against y/δ in Figs. 6a - 6g and one set of profiles for each station are tabulated in Table II. The solid line in each figure is the reference curve $u/U = (y/\delta)^{1/6}$ which agrees with all the profiles upstream of the disturbance (Fig. 6a). The velocity profiles downstream of the corner without any shock (Fig. 6b) also collapse fairly well but the profiles are fuller after accelerating around the corner.

The velocity profiles downstream of the expansion corner with the 6° shock impinging in front, at and behind the corner are compared in Figs. 6f, d and g. In all cases, there is a decrease in fullness of the velocity profiles behind the shock. For the flow with $x_s = -20$ mm, the last four x stations of the velocity profiles ($x > 70$ mm) can be considered as 'near-equilibrium' (quotation marks are used here for reasons to be explained in the following section) since they show a reasonable degree of collapse. For the flow with $x_s = 0$ mm, an 'equilibrium profile' is achieved at about $x = 76.2$ mm. For the flow with $x_s = 20$ mm the last two measuring stations collapse well and flow can be regarded as in 'near-equilibrium' at about 80 mm downstream of the nominal shock impingement position. Thus, irrespective of whether the shock is upstream or downstream of the expansion, the distance necessary for recovery to 'near-equilibrium' flow is about 70 - 80 mm (or approximately 12δ) downstream of the nominal shock impingement position.

Velocity profiles for flows with shocks of $\alpha = 4^{\circ}$, 6° and 8° striking the corner are compared in Figs. 6c, d and e. As expected, the velocity profiles are less full for flows downstream of the stronger shock which leads to a slower relaxation to the 'near-equilibrium' flow. For $\alpha = 4^{\circ}$, the velocity profiles tend to collapse at about 8δ downstream of the corner. For $\alpha = 6^{\circ}$, the collapse occurs at about 12δ downstream of the corner, while for $\alpha = 8^{\circ}$, if

occurs at all, it is greater than 16δ. This eventual collapse of the profiles is clearly shown in Fig. 5b where the variation of H_k with x is plotted. Downstream of the shock impingement point H_k falls rapidly, but then levels out at a level about that in the absence of the shock.

Although the profiles appear to collapse downstream of the shock the final profiles are progressively fuller as the shock impingement position moves upstream, or as the shock becomes weaker. This change in the profiles cannot be accounted for by Mach number and Reynolds number influence alone since the variation of these parameters near the end of the measuring stations is very small. It seems that there is a genuine difference in the turbulence structure between the different experimental configurations although the velocity profiles have collapsed downstream of the corner. The eddies in the boundary layer, after undergoing rapid distortion by the incident shock and/or expansion fan, decay exponentially with time. It is known in incompressible flow that the time constant of decay is a strong function of length scale and local mean-flow gradient (i.e. y/δ). This was also found to be true at hypersonic speed from the hot-wire measurements by Owen et al[12]. (No measurements at supersonic speeds are known to the authors). Thus, the smaller eddies in the inner boundary layer decay faster than the larger eddies in the outer layer. But the overall eddy structure can only be considered to be in true equilibrium when the larger eddies have settled down, since there is a continuous transfer of turbulent energy between the inner and outer layers by advection and diffusion processes. The large scale eddies can take a very long time to decay, e.g. $>> 60\delta$ in hypersonic boundary-layer flow (Owen et al[12]) or 1000 momentum thicknesses in incompressible wake flow (Narasimha and Prabhu[13]).

In addition to the effect of the shock the boundary-layer streamlines are also curved as they pass over the expansion corner. It is known that surface curvature can affect the turbulence structure so part of the change in the shape of the downstream profiles could be due to this effect. Unfortunately it was not possible to produce a shock which exactly cancelled the pressure fall at the corner and so gave a uniform pressure along the plate. However, the pressure disturbance caused by the 4° shock is fairly weak and the pressure far downstream of the corner is close to the upstream value. For this case the downstream value of H_k is just below the upstream value and is the same as that measured in the absence of the shock. Thus it would appear that the effects of curvature are relatively small in this case, and that the main change in the turbulence structure is associated with the shock wave.

This approach to a 'pseudo-equilibrium' profile was also apparent in the experiments of Marriott[7] in which a flat-plate boundary-layer flow was disturbed by fluid injection through a porous plate upstream, and then allowed to recover over a solid plate. Although the velocity profiles collapse reasonably well after about 12δ downstream of the end of injection, the collapsed velocity profiles are different from the ordinary flat-plate boundary-layer profiles at the same value of Re_θ.

5.2 Shear-stress profiles

The shear-stress profiles were derived from the mean flow data as described in section 3.3. As mentioned in that section, there are considerable difficulties in obtaining these profiles and the results can only be used for qualitative purposes.

The normalised shear-stress profiles are plotted against y/δ in Fig. 7. For the flow upstream of the expansion corner the profiles are in qualitative agreement with those for flat-plate boundary-layer flows. The shear stress is nearly constant in the inner boundary layer before tailing off to zero towards the free stream. For the flow downstream of the expansion corner with no impinging shock the acceleration through the Prandtl-Meyer expansion leads to a decrease in turbulence intensity (turbulence intensity is proportional to shear stress according to Townsend[14]) which is in accordance with the literature. The decrease in turbulence intensity is reflected in the drop of the shear stress which relaxes gradually to the flat-plate shear-stress profile as the flow moves downstream.

The shear-stress profiles are compared in Figs. 7f, d and g for flows with the 6° shock impinging in front, at and behind the expansion corner. The computation is rather unstable near the wall where the experimental velocity profiles are more scattered owing to the wall displacement effects and high level of turbulence intensity. In general, the turbulence intensity increases after the boundary layer has gone through a sudden pressure jump. The increase in turbulence intensity is more obvious for x_s = 20 mm where the shear stress is higher. For x_s = -20 mm and 0 mm, the shear-stress profiles do not differ very much from flat-plate situations.

The corresponding shear-stress profiles for shocks of different strength hitting the corner are presented in Figs. 7c, d and e. Although the shear-stress profiles for $\alpha = 4^\circ$ and 6° are approximately similar, there is a distinct increase of the shear stress for $\alpha = 8^\circ$. In this case, the shear stress in the

outer part of the boundary layer does not decrease to the flat-plate level although the wall shear stress has increased and levelled off at the last two measuring stations where the velocity profiles almost collapse. This probably indicates that the eddy structure has not settled down to equilibrium level; but because of the approximate nature of the shear-stress profiles no firm conclusion can be drawn.

5.3 Skin friction and integral parameters

All the integral parameters are tabulated in Table I and the measured momentum developments are plotted in Fig. 5 while the corresponding skin-friction coefficients are plotted in Fig. 8. The figure for the skin friction also includes two theoretical curves. The solid line is the output from an eddy-viscosity calculation and will be discussed below. The dashed line represented the skin friction as predicted by a two-parameter formula developed by Chew[15]. This line is based on the measured values of $R_{\theta i}$ and H_i and is in very good agreement with the measured values.

The other integral parameters basically show the same behaviour as already discussed for the velocity profiles. That is, they show a gradual relaxation to a pseudo-equilibrium form at the end of the development, but with values which do not agree with those for a flat plate boundary layer at the same Mach number and Reynolds number.

5.4 The inner and outer regions of the boundary layer

The boundary layer on a flat plate can conveniently be divided into the inner and outer regions. The inner region consists of small scale eddies and is close to a condition of absolute energy equilibrium, where the local turbulent energy production is nearly dissipated by viscous action. This inner region responds quickly to any changes in local conditions and is heavily influenced by the local wall stress. The outer region consists mostly of larger eddies in which viscous effects are negligible and the production of turbulent energy is small. This gives it a wake-like structure which is responsible for the entrainment of free stream fluid and the boundary-layer growth. The large scale eddies, having a large characteristic time of energy production, are sluggish in response to changes and can carry the upstream history effect for a long distance.

The inner and outer regions are not independent of each other. The mean-flow energy is transferred from the outer to inner region at a rate governed by the Reynolds stress gradient, and the excess turbulent energy produced in the inner region is diffused outward and forms the main source of turbulent energy supply

for the outer region (Townsend[14]). The outer flow contributes most to the derivative of the momentum integral, and it can be seen from the momentum integral equation that the local wall stress depends strongly on the local structure of the outer flow. The local wall stress in turn determines the rate of turbulent energy production near the wall and hence its supply to the outer region. Thus, there is always a continuous transfer of energy between these two regions, and the inner region is not free from the upstream history effect felt by the outer region, although the skin friction may level off as shown in Fig. 8.

In this section, the inner and outer regions will be studied in relation to the law of the wall and defect law. The portion of inner layer next to the wall, being the sublayer where viscous stresses dominate, is not considered since it is too thin to enable any measurements to be made.

5.4.1 Inner region

For flat-plate incompressible flow, the velocity profile in the inner region can be represented by a law of the wall of the form

$$\frac{u}{u_\tau} = \frac{1}{k} \log_e \frac{u_\tau y}{\nu} + B \qquad (4)$$

where k = universal mixing length constant $\doteq 0.41$

B = constant of integration $\doteq 5.0$

Because of the presence of a constant shear stress region in the inner layer of flat-plate flow, eqn. (4) can be derived directly by integrating the Reynolds stress equation using the mixing-length relation of the form

$$\ell = ky \, . \qquad (5)$$

However, for flows with pressure gradient or injection, the shear stress in the inner region is not constant, and the law of the wall and mixing-length theory with k constant are mutually exclusive. If the mixing-length constant is considered as universal (Patel[16]), the velocity profile will depart from the logarithmic law within the whole inner region and there is no wall similarity. If the law of the wall is valid (Galbraith and Head[17]), the existence of a logarithmic law with constant slope implies that k is not a constant. In this case, the effect of pressure gradient or injection is the gradual erosion of the logarithmic portion of velocity profile from the outer edge and the wall similarity near the wall remains.

In spite of the controversy, the bulk of experimental data in the 1968 Stanford Conference Proceedings (Coles and Hirst[18]), supports the existence of

a linear logarithmic region in the velocity profiles for incompressible flows with various type of pressure distributions. For compressible flow, the law of the wall when plotted in Van Driest's transformed velocity, (Appendix A) compares well with the flat-plate experimental data (Lewis, Gran and Kubota[19] White[20]). In fact, it was found that for compressible flows with injection (Squire[21]), and with injection plus favourable or adverse pressure gradient (Thomas[6]), the logarithmic portion of velocity profiles still exists with the slope identical to the flat-plate value.

The experimental data for the seven test configurations in Van Driest's coordinates are plotted in Fig. 9a to Fig. 9g. The seven velocity profiles in each figure are arranged on a staggered ordinate so that the lowest is at the most upstream measuring station. The law of the wall with $k = 0.41$ and $B = 5.0$, as adopted for incompressible flows in the 1968 Stanford Conference Proceedings, is also plotted as continuous straight lines. It can be seen that the profiles upstream of the corner are in good agreement with the low speed law of the wall. This is also true for the flows downstream of the incident shock with an upstream history of an adverse pressure gradient (Figs. 9d, e and g). The adverse pressure gradient is considered as a history effect rather than as a local effect since the local pressure gradient at each profile station is small. The history effect arises from the large upstream pressure rise created by the incident shock which is felt for a long distance downstream and the boundary layer behaves as if it is experiencing a large local pressure gradient. The erosion of the linear logarithmic portion of the velocity profile is large immediately after the interaction regions, but decreases gradually as the boundary layer relaxes towards equilibrium.

The flow downstream of the corner without any incident shock and flows with $\alpha = 6^{o}$, $x_s = -20$ mm or $\alpha = 4^{o}$, $x_s = 0$ mm, resemble flows which have been subjected to favourable pressure gradients. This 'favourable' upstream pressure history effect is carried downstream and reflected in the poorer agreement with the law of the wall in Figs. 9b, 9c, 9f. Generally, the linear logarithmic portions of the velocity profiles are still there, although the experimental data lie at a slightly higher level than the standard law of the wall.

The conclusion that can be drawn from the studies in this section is that the experimental data in the inner region broadly support the existence of a law of the wall; even in these highly non-equilibrium flows with upstream history effects. It should be noted here that the skin friction was measured by Preston tube with Allen's calibration (see section 3.2). Any indirect method of measuring c_f can only be valid if a wall similarity in velocity profiles exists and the obstacle, be it Preston tube, razor blade or etc., is placed

within the wall similarity region. The Preston tube calibration is obtained from flat-plate skin-friction data measured by floating element. Thus, the existence of a law of the wall in flat-plate flow has been implicitly assumed. The calibration curve is then used in the present investigation where the flows are highly non-equilibrium. If there is no wall similarity between these non-equilibrium flows and flat-plate flow, the calibration curve which implies the existence of a law of the wall in flat-plate flow would yield results which do not agree with the logarithmic law. However, the present data do lie on the logarithmic law and support the wall similarity between equilibrium and non-equilibrium flows. Hence, the findings here support the existence of a universal law of the wall for both equilibrium and non-equilibrium flows; rather than being the consequence of measuring skin friction with the Preston tube.

The maximum height of the Preston tube is marked as a vertical arrow in each of the Figs. 9a - g. It can be seen that even for flows with strong incident shock as in Fig. 9e the Preston tube is within the wall similarity portion of velocity profiles, and the use of this method for measuring c_f in the highly non-equilibrium flows is justifiable.

5.4.2 Outer region

The velocity defect law for an incompressible flat-plate boundary layer is usually written as

$$\frac{U - u}{u_\tau} = f\left(\frac{y}{\delta}\right) \quad . \tag{6}$$

For compressible flat-plate adiabatic flow, Maise and McDonald[21] found that if the Van Driest's transformed velocity is used in eqn. (6), the velocity profiles at different Mach numbers are well correlated by

$$\frac{U_i - u_i}{u_\tau} = f\left(\frac{y}{\delta}\right) \quad . \tag{7}$$

It was found that the profiles upstream of the corner did collapse onto a single curve when plotted as in eqn. (7), but no collapse was found downstream of the corner even when no shock was present.

When the boundary layers are disturbed by an incident shock, eqn. (7) is not valid for it does not take the pressure gradient into account. Even if the pressure gradient is taken into account, it cannot describe the present flows since the pressure gradient felt by the boundary layers is entirely an upstream history effect. There is insufficient understanding about how the upstream history effect can be accounted for and so no effort is made to collapse the data onto a defect law.

Alternatively, the outer region can be studied by considering the boundary-layer velocity profile as the sum of the logarithmic inner velocity profile represented by the law of the wall and the outer wake-like component represented by the deviation from the law of the wall. The incompressible velocity profile family representing both the inner and outer regions (neglecting the viscous sublayer) as proposed by Coles[23] is then

$$\frac{u}{u_\tau} = \frac{1}{k} \log_e y^+ + B + \frac{\pi}{k} w\left(\frac{y}{\delta}\right) \tag{8}$$

where π is the wake parameter and w the wake function. k and B take the same values as in eqn. (4) and the wake function can be approximated by

$$w\left(\frac{y}{\delta}\right) = 2 \sin^2\left(\frac{\pi}{2} \frac{y}{\delta}\right) \tag{9}$$

which agrees well with various experimental data (Coles and Hirst[18]). Eqn. (8) can be used for compressible flow if the measured velocity is replaced by the transformed velocity.

The compressible form of eqn. (8) is plotted in Figs. 9a to 9g as the solid curves. As little is known about the behaviour of π in compressible flow with a pressure gradient (not to mention the present flows with upstream history effect), π is obtained empirically from the experimental data. The curves fit the experimental data for flows upstream of the expansion corner well. For flows downstream of the incident shock in Figs. 9d, 9e and 9g, where the law of the wall agrees well with the experimental data, the fits are still fair except for flows with very strong wakes. However, when the profiles do not agree with the law of the wall the agreement with the wake law is also poor.

6. COMPARISON OF THE MEASURED PROFILES WITH CALCULATION

In this section all the measured profiles are compared first with the predictions from a calculation method based on eddy viscosity. The eddy viscosity model used is similar to that suggested by Cebeci and Smith[24] and is defined in Appendix B. The actual calculation method used is that developed by Verma[25]. As will be seen this method did not give satisfactory predictions of the flow development downstream of the strong interactions and so further comparisons were made for some of the profiles with predictions from Bradshaw's[26] method. The results were again unsatisfactory and so attempts were made to improve the predictions from the eddy-viscosity model. The results of these modifications are described in the last part of this section.

6.1 Predictions from the eddy-viscosity model

The predicted velocity profiles from Verma's method* are plotted as solid lines in Figs. 10a - 10g. All these profiles were calculated with the initial profile taken as equal to the profile at the first upstream station, and with the pressure distribution taken from the measured wall pressures. This enabled the calculation to march through the interaction region.

As expected the calculated profiles are in good agreement with the measured profiles upstream of the corner (Fig. 10a). The agreement is also good for the flow downstream of the expansion corner without a shock (Fig. 10b). For flows with an incident shock of 6° deflection angle hitting in front, behind or at the corner in Figs. 10f, 10g and 10d, the predictions are good when the shock is in front of the corner. As the shock moves towards the corner and closer to the downstream measuring stations, the predictions deteriorate, although the discrepancies between the predicted curves and the experimental data decrease and disappear eventually further downstream.

When the shocks of different strength hit the corner, agreement is good when the shock is weak, but deteriorates as the shock becomes stronger. At $\alpha = 8^{\circ}$ (Fig. 10e), the discrepancies are very large indeed, but the predicted curves and experimental profiles begin to assume similar shapes at about $x = 76.2$ mm.

The skin-friction predictions (Fig. 8) follow the trends of experimental data well, although in all cases downstream of the interaction regions the predicted levels are high. Even for the highly non-equilibrium flow at $\alpha = 8^{\circ}$, the prediction manages to reproduce the sudden dip in c_f at the shock impingement position before relaxing to the near constant values further downstream, although it does not predict separation. For flows upstream of the interaction regions, the predictions are good as expected.

Generally, it can be concluded that Verma's method is able to predict the development of the boundary layer across a Prandtl-Meyer expansion with turning angle up to 6° reasonably well. When the boundary-layer flow is disturbed by an incident shock, the prediction is still reasonable if the disturbance is weak, but deteriorates rapidly as the shock strength increases. Whatever the form of disturbances in the interaction regions, the predicted and measured boundary-layer developments finally merge far downstream.

6.2 Bradshaw's method

In order to compare the eddy-viscosity method with others using a

---

* For convenience the eddy viscosity calculation is referred to as Verma's method

completely different approach, Bradshaw's method was used to compute the boundary-layer development for $M = 2.5$, $\alpha = 8^{\circ}$, $x_s = 0$ mm which is the most difficult case to predict in the present investigation. The results are plotted in chain line.

The predicted velocity profiles upstream of the incident shock are compared with the experimental data in Fig. 10a. The agreement is not as good as that from Verma's method although the discrepancies are not large. The predicted profiles downstream of the corner are plotted in Fig. 10e. They are rather irregular, and a distinct kink is present near the wall. This is presumably the consequence of using the method of characteristics in which upstream influences are propagated along characteristics. Similar behaviour was also observed by Marriott[7] when Bradshaw's method was used to predict the highly non-equilibrium boundary layer developments downstream of a change in surface injection. In spite of the irregularities in the predicted profiles, they are generally close to the curves predicted by Verma's method.

6.3 Modifications to the eddy-viscosity model

The inner and outer forms of the eddy viscosity used by Verma are defined in Appendix B and these forms are known to be adequate for moderate pressure gradients and small injection rates. However, they are clearly inadequate for the highly non-equilibrium flows considered here. A number of modifications were made to the basic form of the eddy viscosity and the results were compared with the measured flow generated by the 8° shock striking the surface at the corner (case e).

The first modification simply followed the suggestion of Galbraith and Head[17] that the constant k in the mixing length be replaced by an effective $\bar{k}$ defined by

$$\bar{k} = k(\tau/\tau_w)^{\frac{1}{2}} \doteq k(1 + y^+p^+)^{\frac{1}{2}} . \qquad (10)$$

It was found that the numerical scheme became unstable and the solution did not converge except for very small values of p^+. A similar type of behaviour was found by Smith[27] in his work on shock-wave/boundary-layer interactions downstream of injection. For adverse pressure gradients the modification in eqn. (10) increases k and a similar increase can be achieved by the introduction of the correction for bulk dilatation as suggested by Bradshaw[28]. He divided the dissipation term in his calculation method by a factor F given by

$$F = 1 - E\frac{\text{div } u}{\partial u/\partial y} = 1 + E\frac{u}{\gamma p}\frac{dp}{dx}\Big/\frac{\partial u}{\partial y} \qquad (11)$$

where E is a constant of order 10. To a local-equilibrium approximation this

correction is equivalent to multiplying the mixing length in Verma's method by F, i.e. k is again increased in adverse gradients. This modification was incorporated into Verma's program but the solution would only converge for $E < 3$, and the overall effect on the solution was small.

These changes can only affect the inner part of the layer, whereas Fig. 10 shows that the wake component of the calculated profile is too small just downstream of the interaction. This wake component can be increased if the constant c_o in the outer form of the eddy viscosity is decreased (Squire and Verma[29]) and Kuhn and Nielson[30] have produced such a reduction by the formula

$$c_o = 0.013 + 0.0038e^{-p_k^x/15}, \quad \text{where} \quad p_k^x = \frac{\delta_k^*}{\tau_w}\frac{dp}{dx} \quad . \tag{12}$$

Use of this form for c_o moved the profiles slightly closer to the measured profiles, but the effect was short lived since no lag equation was included.

A lag equation has been developed from the work of Rose and Johnson[31] who measured the fluctuating velocities upstream and downstream of a shock/boundary-layer interaction using hot wires and a laser system. From their measurements they found that the turbulence remains almost constant across the interaction before relaxing further downstream. As a result they suggested that the eddy viscosity in the outer part of the layer should take the same value immediately upstream and downstream of the interaction and that it should be allowed to relax to the local value with a relaxation distance of about 10δ. This model was used successfully by Murphy et al[32] and by Shang and Hankey[33]. In the present investigation it was found that the calculated profiles moved closer to the measured profiles, but the movement was still not big enough.

In a final attempt to test if it was possible to improve the present method by changes in c_o it was decided to give c_o the following form:

$$c_o = 0.0168 \quad \text{for} \quad x < -3.5 \text{ mm} \quad \text{(i.e. upstream of the interaction)}$$

$$c_o = 0.004 \quad \text{for} \quad -3.5 \leq x \leq 19 \quad \text{(the interaction region)}$$

$$c_o = 0.004 + 0.0128\,(1 - \exp((19 - x)/3\delta)), \quad x > 19 \text{ mm}. \tag{13}$$

The results of this modification are plotted in Fig. 10e, and it will be seen that the overall improvement is small. It must be concluded that most of the discrepancies arise from the failure of the prediction method in the interaction region itself.

In order to examine the performance of Verma's method if its shortcoming in the interaction region was absent, calculations were made with, and without, the above modifications using the first profile measured downstream of the interaction as input. The results of these comparisons are presented in Fig. 11.

For the unmodified results, the relaxation to equilibrium is too rapid and discrepancies begin to appear at the second profile, although the calculated and measured profiles are in good agreement far downstream. With the modifications defined by eqns. (11) and (13) the relaxation is slowed down and the agreement is much improved.

7. CONCLUSIONS

The main results of this investigation may be summarised as follows -

1) The velocity profile after being disturbed by an incident shock relaxes in an asymptotic fashion to a 'near-equilibrium' form. The relaxation distance is virtually independent of whether the shock impingement position is in front, at or behind the expansion corner. However, it increases with increasing shock strength, so that for 4° and 6° shocks the relaxation distances are approximately 8δ and 12δ respectively, while for the 8° shock the relaxation distance is greater than 16δ.

2) For flows with different upstream pressure history the collapsed velocity profiles are not identical. The discrepancies cannot be explained by Mach number or Reynolds number effects alone and are attributed to upstream history effect. Thus, the rapid collapse of velocity profiles may only indicate the reaching of a 'pseudo-equilibrium' flow where the initial rapid distortion of the large eddies by the incident shock has disappeared.

3) In spite of the discrepancies between the centreline and off-centreline pressure distributions downstream of the incident shock, the departure from two-dimensionality of the downstream velocity profiles, measured along the centreline, is in no case very great. This is supported by the momentum thickness calculated from the two-dimensional momentum integral equation, the oil-flow visualisation studies and the static pressure profile measurements.

4) The inner velocity profiles, when transformed into incompressible form according to Van Driest's transformation and plotted on the semi-logarithmic plot, broadly support the existence of a logarithmic law; even for the highly non-equilibrium flows. This implies wall similarity between the equilibrium and non-equilibrium flows, and supports the validity of using a Preston tube for skin-friction measurement: provided that its diameter is within the wall-similarity portion of velocity profile.

5) The outer velocity profiles for flows without an incident shock support the defect law when plotted in Van Driest's transformed velocity coordinates. The profiles for flows with incident shocks are also broadly in agreement with Coles' wake law if π is taken as a free parameter.

5) Verma's eddy viscosity method is able to predict the boundary-layer development for flows with weak incident shocks in the present investigation. However, when the incident shock is strong it does not predict the boundary-layer development downstream of the interaction region accurately. This is due to its failure to predict the first profile downstream of the interaction region correctly since the boundary-layer approximation is no longer valid in the strong interaction region.

6) When the first measured profile downstream of the interaction region is used as the initial input to Verma's method, the prediction is fair. It manages to reveal the relaxation of c_f and the velocity profile to 'near-equilibrium' level although the predicted relaxation is slightly faster than the experimental results.

7) The inner eddy-viscosity model adopted in Verma's method was modified by Bradshaw's dilatation correction. This has the effect of increasing the mixing-length 'constant' gradually away from the wall for flow with adverse pressure gradient and brings the velocity profile in the inner region closer to the logarithmic law. The modification has no appreciable effect on the other parameters except to increase the level of c_f slightly. It also has the tendency of de-stabilising the numerical algorithm.

8) The outer-eddy-viscosity model adopted in Verma's method was modified by decreasing the constant of proportionality, c_o, in the eddy viscosity in the outer part of the layer to a low level just after the interaction region and before it relaxed exponentially to the equilibrium value. This has the effect of increasing the wake component and includes the transport properties of turbulence as a first order approximation in order to account for the history effect. The modification decreases the skin-friction level, delays the relaxation of velocity profile to 'near-equilibrium' shape and hence improves the agreement between the predicted and experimental results. The computation is stable with this modification.

APPENDIX A

Definition of the integral parameters

In addition to the normal momentum and displacement thicknesses defined by

$$\theta = \int_o^\infty \frac{\rho u}{\rho_1 U}\left(1 - \frac{u}{U}\right)dy, \quad \delta^* = \int_o^\infty \left(1 - \frac{\rho u}{\rho_1 U}\right)dy \tag{A.1}$$

a number of other integral parameters were calculated. These are defined as follows.

1) Kinematic parameters

$$\theta_k = \int_o^\infty \frac{u}{U}\left(1 - \frac{u}{U}\right)dy, \quad \delta_k^* = \int_o^\infty \left(1 - \frac{u}{U}\right)dy \quad . \tag{A.2}$$

2) 'Incompressible parameters'

The incompressible parameters were obtained by first transforming the velocity to incompressible form by Van Driest's transformation

$$u_i = \int_o^u \left(\frac{\rho}{\rho_w}\right)^{\frac{1}{2}} du' = \int_o^u \left(\frac{T_w}{T}\right)^{\frac{1}{2}} du' \tag{A.3}$$

where u_i was obtained by numerical integration using the assumed temperature from the Crocco relation (eqn. (1)). The corresponding parameters were then defined as

$$\theta_i = \int_o^\infty \frac{u_i}{U_i}\left(1 - \frac{u_i}{U_i}\right)dy, \quad \delta_i^* = \int_o^\infty \left(1 - \frac{u_i}{U_i}\right)dy \tag{A.4}$$

APPENDIX B

Eddy-viscosity model

1) Inner region $\quad \nu_t = k^2 y^2 \left[1 - \exp\left(-\frac{y^+}{A^+}\right)^2\right] \left|\frac{\partial u}{\partial y}\right|$

where $k = 0.4$

$$A^+ = 26\left(1 + 11.8\, p^+\right)^{-\frac{1}{2}}$$

$$p^+ = \frac{\nu}{\rho_w u_\tau^3}\frac{dp}{dx}$$

2) Outer region $\quad \nu_t = c_o U \delta_k^* / \left(1 + 5.5\,(y/\delta)^6\right)$

where $c_o = 0.0168$ for standard calculations.

TABLE I

INTEGRAL PARAMETERS

X	M	R_θ	$c_f \times 10^3$	θ	δ^*	H	θ_k	δ_k^*	θ_i	δ_i^*
CASE a. Flow upstream of corner										
-101.6	2.559	20300	1.38	0.404	1.692	4.19	0.582	0.790	0.656	0.942
-101.6	2.561	20500	1.36	0.410	1.725	4.21	0.588	0.799	0.664	0.952
-76.2	2.534	20700	1.35	0.422	1.708	4.05	0.596	0.800	0.676	0.954
-76.2	2.534	20800	1.34	0.426	1.716	4.03	0.598	0.801	0.669	0.946
-50.8	2.535	21900	1.38	0.442	1.799	4.07	0.625	0.836	0.704	0.994
-50.8	2.534	21700	1.38	0.439	1.784	4.07	0.621	0.833	0.702	0.993
-38.1	2.524	22800	1.35	0.459	1.855	4.04	0.648	0.869	0.733	1.033
-38.1	2.520	22800	1.38	0.461	1.868	4.05	0.654	0.883	0.736	1.046
-25.4	2.530	23800	1.34	0.474	1.916	4.05	0.669	0.895	0.754	1.062
-25.4	2.531	23800	1.36	0.474	1.929	4.07	0.673	0.906	0.759	1.077
-12.7	2.500	23200	1.36	0.469	1.869	3.99	0.657	0.877	0.741	1.041
-12.7	2.497	23300	1.37	0.469	1.870	4.01	0.657	0.878	0.743	1.046
-6.4	2.513	24500	1.34	0.485	1.939	3.99	0.680	0.902	0.770	1.074
-6.4	2.510	24500	1.34	0.488	1.950	4.00	0.685	0.913	0.771	1.084
CASE b. Flow downstream of corner, no shock.										
19.0	2.759	23400	1.34	0.520	2.294	4.41	0.735	0.937	0.862	1.152
19.0	2.763	24600	1.33	0.530	2.392	4.48	0.758	0.970	0.886	1.191
25.4	2.804	26200	1.31	0.558	2.570	4.60	0.808	1.038	0.958	1.293
25.4	2.794	26300	1.31	0.565	2.560	4.53	0.814	1.052	0.956	1.295
38.1	2.809	26300	1.28	0.576	2.638	4.58	0.831	1.074	0.997	1.345
38.1	2.786	25500	1.28	0.563	2.549	4.53	0.810	1.046	0.948	1.285
50.8	2.776	22500	1.30	0.523	2.357	4.51	0.752	0.982	0.880	1.205
50.8	2.771	22400	1.27	0.513	2.298	4.48	0.734	0.950	0.862	1.171
76.2	2.859	24100	1.27	0.549	2.592	4.72	0.806	1.045	0.950	1.295
76.2	2.868	25000	1.23	0.557	2.614	4.69	0.808	1.037	0.959	1.289
101.6	2.728	23800	1.21	0.567	2.497	4.40	0.812	1.060	0.944	1.293
101.6	2.727	23700	1.20	0.565	2.490	4.41	0.810	1.058	0.941	1.290
127.0	2.844	26900	1.17	0.598	2.787	4.66	0.873	1.134	1.024	1.394
127.0	2.843	27100	1.17	0.605	2.809	4.65	0.883	1.141	1.036	1.409
CASE c. Flow downstream of corner, 4° shock at corner										
19.0	2.339	26700	1.11	0.506	1.880	3.72	0.697	0.966	0.771	1.119
19.0	2.351	27700	1.11	0.517	1.925	3.72	0.710	0.976	0.787	1.134
25.4	2.442	31100	1.01	0.530	2.079	3.92	0.735	1.053	0.832	1.226
25.4	2.425	31900	1.02	0.536	2.102	3.92	0.761	1.061	0.843	1.239
38.1	2.407	26300	1.15	0.479	1.956	4.08	0.658	0.913	0.849	1.209
38.1	2.406	29400	1.18	0.538	2.044	3.80	0.746	1.017	0.832	1.187
50.8	2.459	29900	1.21	0.555	2.134	3.85	0.763	0.999	0.865	1.197
50.8	2.456	29300	1.21	0.543	2.086	3.84	0.749	0.983	0.844	1.169
76.2	2.450	26400	1.26	0.519	1.964	3.79	0.705	0.908	0.796	1.078
76.2	2.457	26800	1.26	0.521	1.987	3.81	0.710	0.916	0.804	1.083
101.6	2.484	27000	1.19	0.524	2.004	3.83	0.713	0.914	0.808	1.086
101.6	2.491	28300	1.20	0.536	2.076	3.87	0.736	0.958	0.825	1.111
127.0	2.495	31200	1.18	0.587	2.272	3.91	0.811	1.060	0.923	1.264
127.0	2.492	30100	1.20	0.570	2.234	3.92	0.783	1.007	0.916	1.253

TABLE I (continued)

X	M	R_θ	$c_f \times 10^3$	θ	δ^*	H	θ_k	δ^*_k	θ_i	δ^*_i
CASE d. Flow downstream of corner, 6° shock at corner.										
19.0	2.198	35000	0.83	0.579	2.181	3.77	0.826	1.285	0.883	1.445
19.0	2.203	35600	0.83	0.577	2.197	3.80	0.827	1.286	0.885	1.451
25.4	2.267	40800	0.86	0.629	2.431	3.86	0.908	1.388	0.975	1.566
25.4	2.266	40900	0.87	0.634	2.446	3.86	0.914	1.400	0.981	1.578
38.1	2.256	36100	1.07	0.611	2.271	3.71	0.862	1.258	0.933	1.428
38.1	2.259	36900	1.09	0.616	2.306	3.74	0.871	1.269	0.944	1.448
50.8	2.268	32200	1.19	0.579	2.117	3.65	0.805	1.139	0.879	1.287
50.8	2.270	32300	1.20	0.579	2.113	3.65	0.804	1.141	0.875	1.281
76.2	2.318	30800	1.23	0.568	2.051	3.61	0.775	1.043	0.854	1.202
76.2	2.321	30900	1.23	0.567	2.081	3.67	0.777	1.062	0.864	1.217
101.6	2.312	32700	1.28	0.604	2.164	3.58	0.817	1.092	0.910	1.273
101.6	2.308	32700	1.28	0.602	2.163	3.60	0.818	1.097	0.906	1.275
127.0	2.291	34000	1.27	0.624	2.234	3.58	0.847	1.140	0.935	1.309
127.0	2.293	34500	1.30	0.633	2.257	3.57	0.858	1.151	0.948	1.333
CASE e. Flow downstream of corner, 8° shock at corner										
19.0	2.067	39900	0.31	0.661	2.764	4.18	0.966	1.909	0.992	2.078
19.0	2.067	41100	0.32	0.669	2.796	4.18	0.977	1.934	0.997	2.109
25.4	2.082	44200	0.45	0.707	2.825	3.99	1.038	1.874	1.055	2.111
25.4	2.080	42600	0.45	0.684	2.903	4.24	0.999	2.004	1.057	2.111
38.1	2.078	41700	0.76	0.697	2.626	3.77	0.996	1.691	1.045	1.844
38.1	2.071	41300	0.75	0.683	2.616	3.83	0.985	1.701	1.036	1.838
50.8	2.119	41100	0.98	0.691	2.511	3.63	0.974	1.541	1.032	1.679
50.8	2.117	40800	0.98	0.684	2.516	3.68	0.968	1.546	1.024	1.674
76.2	2.172	39400	1.22	0.680	2.380	3.50	0.936	1.345	1.008	1.509
76.2	2.181	40100	1.19	0.674	2.402	3.57	0.935	1.357	1.006	1.506
101.6	2.157	40700	1.27	0.700	2.372	3.39	0.943	1.314	1.024	1.488
101.6	2.164	41700	1.26	0.711	2.425	3.41	0.960	1.343	1.041	1.516
127.0	2.126	44200	1.28	0.759	2.507	3.30	1.009	1.382	1.095	1.567
127.0	2.125	44200	1.29	0.757	2.516	3.33	1.008	1.392	1.098	1.584
CASE f. Flow downstream of corner, 6° shock 20 mm upstream of corner										
19.0	2.255	33100	1.26	0.578	2.108	3.64	0.798	1.127	0.889	1.305
19.0	2.252	31900	1.25	0.563	2.071	3.68	0.774	1.115	0.878	1.285
25.4	2.281	33900	1.28	0.591	2.135	3.61	0.817	1.132	0.893	1.299
25.4	2.280	33300	1.29	0.590	2.139	3.62	0.817	1.136	0.893	1.302
38.1	2.279	31500	1.32	0.576	2.064	3.58	0.788	1.073	0.864	1.231
38.1	2.280	31500	1.31	0.573	2.047	3.57	0.781	1.068	0.860	1.224
50.8	2.306	33300	1.36	0.611	2.208	3.61	0.835	1.137	0.914	1.280
50.8	2.307	33100	1.30	0.597	2.157	3.61	0.813	1.086	0.903	1.261
76.2	2.306	33400	1.28	0.601	2.163	3.60	0.815	1.078	0.904	1.262
76.2	2.307	33700	1.24	0.615	2.180	3.54	0.829	1.100	0.918	1.272
101.6	2.270	35500	1.30	0.654	2.278	3.48	0.875	1.157	0.971	1.351
101.6	2.269	35500	1.31	0.652	2.280	3.50	0.874	1.159	0.970	1.357
127.0	2.269	37800	1.30	0.680	2.372	3.49	0.907	1.193	1.008	1.386
127.0	2.264	37300	1.29	0.680	2.339	3.44	0.902	1.186	0.999	1.372

TABLE I (concluded)

X	M	R_θ	$c_f \times 10^3$	θ	δ^*	H	θ_k	δ^*_k	θ_i	δ^*_i
CASE g. Flow downstream of corner, 6° shock 20 mm downstream of corner										
31.8	2.239	34000	0.37	0.600	2.439	4.07	0.871	1.485	0.914	1.681
31.8	2.239	34300	0.38	0.600	2.502	4.17	0.875	1.551	0.925	1.722
38.1	2.210	35500	0.51	0.610	2.427	3.98	0.893	1.482	0.934	1.691
38.1	2.211	34900	0.52	0.601	2.429	4.04	0.880	1.505	0.924	1.688
50.8	2.186	36500	0.81	0.642	2.426	3.78	0.920	1.451	0.975	1.646
50.8	2.187	36500	0.82	0.643	2.465	3.83	0.928	1.493	0.982	1.671
63.5	2.249	37200	1.03	0.644	2.527	3.77	0.920	1.363	0.993	1.559
63.5	2.244	36300	1.02	0.637	2.364	3.71	0.901	1.301	0.986	1.542
76.2	2.277	35400	1.14	0.634	2.364	3.73	0.898	1.313	0.970	1.466
76.2	2.278	35300	1.13	0.632	2.360	3.74	0.893	1.306	0.966	1.457
101.6	2.325	35500	1.24	0.632	2.360	3.73	0.883	1.219	0.975	1.408
101.6	2.323	35200	1.24	0.642	2.370	3.69	0.894	1.235	0.982	1.424
127.0	2.308	35100	1.25	0.637	2.334	3.66	0.881	1.216	0.967	1.384
127.0	2.308	35100	1.24	0.641	2.337	3.65	0.885	1.218	0.971	1.391

NOTE: All dimensions in millimetres.

Table II

VELOCITY PROFILES

(a) Upstream of corner

X = -101.6		X = -76.2		X = -50.8		X = -38.1		X = -25.4		X = -12.7		X = -6.4	
Y	u/U	Y	u/U	Y	u/U	Y	u/U	Y	u/U	Y	u/U	Y	u/U
0.0	0.0	0.0	0.0	0.0	0.0	0.0	0.0	0.0	0.0	0.0	0.0	0.0	0.0
0.09	0.529	0.09	0.532	0.09	0.528	0.09	0.514	0.09	0.523	0.09	0.516	0.09	0.535
0.20	0.573	0.12	0.570	0.19	0.574	0.19	0.593	0.16	0.569	0.17	0.576	0.22	0.608
0.33	0.619	0.28	0.628	0.29	0.632	0.33	0.636	0.29	0.625	0.29	0.632	0.33	0.654
0.49	0.678	0.43	0.674	0.41	0.675	0.54	0.693	0.45	0.670	0.43	0.676	0.50	0.693
0.74	0.725	0.64	0.713	0.62	0.712	0.79	0.731	0.68	0.712	0.67	0.715	0.79	0.726
1.02	0.761	0.94	0.751	0.89	0.744	1.14	0.761	1.09	0.754	1.11	0.758	1.14	0.757
1.48	0.799	1.38	0.788	1.26	0.775	1.57	0.791	1.64	0.791	1.52	0.788	1.57	0.785
1.88	0.826	1.81	0.816	1.56	0.796	2.05	0.821	2.06	0.822	1.69	0.816	1.99	0.816
2.38	0.859	2.33	0.855	1.97	0.823	2.41	0.849	2.58	0.851	2.39	0.844	2.45	0.845
2.80	0.886	2.75	0.880	2.39	0.648	2.91	0.876	3.02	0.877	2.77	0.866	2.98	0.871
3.16	0.908	3.10	0.902	2.74	0.873	3.34	0.901	3.49	0.904	3.15	0.887	3.32	0.895
3.55	0.934	3.47	0.924	3.17	0.897	3.85	0.925	3.98	0.928	3.58	0.910	3.77	0.915
3.98	0.954	3.83	0.941	3.49	0.916	4.31	0.946	4.48	0.947	4.01	0.929	4.27	0.935
4.38	0.972	4.14	0.959	3.84	0.933	4.75	0.965	4.97	0.968	4.38	0.946	4.74	0.955
4.78	0.986	4.65	0.979	4.16	0.948	5.38	0.985	5.45	0.985	4.79	0.963	5.16	0.972
5.58	0.996	5.19	0.993	4.57	0.966	6.25	0.998	6.27	0.997	5.24	0.979	5.72	0.985
7.01	1.001	6.88	0.999	5.09	0.983	8.10	1.000	7.55	1.000	5.95	0.993	6.55	0.996
8.87	1.000	8.91	0.999	5.69	0.995					6.91	1.000	8.16	0.998
				6.95	1.000							9.80	1.000

(b) Downstream of corner, no shock

X = 19.0		X = 25.4		X = 38.1		X = 50.8		X = 76.2		X = 101.6		X = 127.0	
Y	u/U	Y	u/U	Y	u/U	Y	u/U	Y	u/U	Y	u/U	Y	u/U
0.0	0.0	0.0	0.0	0.0	0.0	0.0	0.0	0.0	0.0	0.0	0.0	0.0	0.0
0.09	0.528	0.09	0.515	0.09	0.497	0.09	0.497	0.09	0.503	0.09	0.497	0.09	0.501
0.15	0.607	0.19	0.573	0.20	0.575	0.17	0.561	0.25	0.587	0.21	0.576	0.19	0.583
0.23	0.648	0.30	0.640	0.36	0.647	0.36	0.632	0.42	0.673	0.40	0.651	0.36	0.648
0.40	0.695	0.42	0.681	0.57	0.703	0.49	0.677	0.59	0.718	0.63	0.701	0.68	0.703
0.62	0.750	0.61	0.723	0.81	0.745	0.60	0.707	0.88	0.747	0.96	0.741	1.09	0.747
1.03	0.791	0.94	0.765	1.39	0.788	0.88	0.749	1.35	0.783	1.36	0.777	1.69	0.794
1.90	0.826	1.63	0.801	2.23	0.831	1.17	0.782	1.79	0.810	1.86	0.811	2.42	0.831
2.62	0.855	2.39	0.839	3.32	0.871	1.86	0.818	2.38	0.837	2.36	0.836	3.06	0.859
3.37	0.882	3.21	0.868	4.31	0.902	2.39	0.842	3.22	0.867	3.03	0.863	3.90	0.888
4.19	0.910	4.06	0.896	5.09	0.926	2.87	0.871	4.03	0.899	3.70	0.888	4.70	0.912
4.92	0.933	4.84	0.921	5.98	0.949	3.54	0.895	4.73	0.921	4.23	0.906	5.52	0.931
5.59	0.952	5.59	0.941	6.92	0.970	4.15	0.913	5.40	0.938	4.99	0.926	6.35	0.950
6.24	0.969	6.37	0.962	7.92	0.986	4.65	0.930	6.11	0.955	5.61	0.948	7.19	0.968
6.96	0.984	7.11	0.978	9.60	0.995	5.31	0.946	6.73	0.970	6.28	0.958	8.05	0.981
8.03	0.998	7.99	0.991	11.82	0.999	5.86	0.960	7.45	0.984	7.05	0.975	8.76	0.991
8.51	1.000	9.90	0.997	13.94	0.998	6.61	0.976	8.31	0.994	7.75	0.987	9.56	0.997
		11.97	1.000	16.14	0.998	7.38	0.988	9.66	0.999	8.57	0.997	10.19	1.000
				18.10	1.000	8.44	0.997			9.90	1.000	11.05	1.000
						9.47	0.999						
						11.34	1.000						

(c) Downstream of corner, 4° shock at corner

X = 19.0		X = 25.4		X = 38.1		X = 50.8		X = 76.2		X = 101.6		X = 127.0	
Y	u/U	Y	u/U	Y	u/U	Y	u/U	Y	u/U	Y	u/U	Y	u/U
0.0	0.0	0.0	0.0	0.0	0.0	0.0	0.0	0.0	0.0	0.0	0.0	0.0	0.0
0.09	0.493	0.09	0.461	0.09	0.492	0.09	0.580	0.09	0.614	0.09	0.614	0.09	0.505
0.20	0.553	0.13	0.526	0.10	0.570	0.39	0.633	0.29	0.674	0.21	0.674	0.12	0.562
0.41	0.612	0.39	0.584	0.45	0.629	0.50	0.680	0.53	0.722	0.50	0.714	0.21	0.633
0.70	0.664	0.61	0.634	0.68	0.670	0.98	0.728	0.92	0.749	0.69	0.741	0.44	0.677
0.98	0.714	0.89	0.680	0.99	0.720	1.43	0.765	1.45	0.783	1.24	0.775	0.58	0.712
1.39	0.752	1.19	0.722	1.51	0.757	1.99	0.801	1.98	0.815	1.68	0.800	1.03	0.747
1.75	0.787	1.73	0.765	2.06	0.797	2.53	0.831	2.42	0.840	2.09	0.825	1.58	0.778
2.36	0.827	2.21	0.796	2.63	0.832	2.96	0.857	2.92	0.862	2.71	0.850	2.17	0.809
2.76	0.859	2.62	0.828	3.17	0.861	3.52	0.884	3.40	0.887	3.21	0.875	2.78	0.834
3.30	0.890	3.08	0.857	3.56	0.884	4.00	0.905	3.99	0.914	3.60	0.891	3.35	0.862
3.81	0.922	3.52	0.886	4.08	0.911	4.47	0.924	4.30	0.923	3.99	0.911	3.87	0.884
4.31	0.944	3.98	0.910	4.54	0.933	4.93	0.941	4.73	0.941	4.49	0.928	4.49	0.909
4.80	0.966	4.30	0.930	5.03	0.953	5.29	0.959	5.05	0.953	4.89	0.942	4.96	0.927
5.35	0.983	4.67	0.947	5.57	0.978	6.00	0.975	5.51	0.968	5.45	0.962	5.51	0.945
6.27	0.995	5.02	0.963	6.08	0.988	6.49	0.987	5.96	0.980	5.89	0.976	6.00	0.963
7.23	0.996	5.24	0.976	6.98	0.993	7.22	0.993	6.51	0.992	6.39	0.986	6.61	0.977
8.29	0.999	5.57	0.956	8.06	0.999	7.98	0.996	7.08	0.998	7.08	0.996	7.37	0.991
9.29	1.000	6.22	0.994	9.17	1.000	9.04	0.997	7.98	1.000			8.82	1.000
		6.96	0.994			10.06	0.999						
		7.90	1.000										

Table II (continued)

(d) Downstream of corner, 6° shock at corner

X = 19.0		X = 25.4		X = 38.1		X = 50.8		X = 76.2		X = 101.6		X = 127.0	
Y	u/U	Y	u/U	Y	u/U	Y	u/U	Y	u/U	Y	u/U	Y	u/U
0.0	0.0	0.0	0.0	0.0	0.0	0.0	0.0	0.0	0.0	0.0	0.0	0.0	0.0
0.09	0.395	0.09	0.412	0.09	0.457	0.09	0.505	0.09	0.534	0.09	0.511	0.09	0.511
0.30	0.435	0.23	0.476	0.22	0.534	0.11	0.562	1.11	0.729	0.11	0.563	0.12	0.573
0.58	0.483	0.49	0.523	0.51	0.582	0.36	0.612	1.67	0.759	0.31	0.613	0.23	0.619
0.63	0.542	0.89	0.577	0.87	0.621	0.72	0.653	2.11	0.791	0.40	0.655	0.48	0.663
1.14	0.614	1.23	0.622	1.22	0.658	1.20	0.693	2.64	0.820	0.63	0.689	0.87	0.707
1.63	0.682	1.77	0.684	1.71	0.704	1.71	0.733	3.08	0.848	1.01	0.723	1.38	0.742
2.13	0.739	2.28	0.735	2.32	0.760	2.11	0.766	3.44	0.870	1.53	0.757	1.91	0.774
2.56	0.782	2.99	0.797	2.98	0.817	2.46	0.794	3.74	0.889	2.14	0.791	2.52	0.806
3.00	0.821	3.71	0.857	3.61	0.864	2.84	0.821	4.11	0.908	2.71	0.822	3.05	0.832
3.41	0.855	4.46	0.910	4.44	0.917	3.22	0.848	4.62	0.932	3.29	0.852	3.55	0.858
4.06	0.905	5.03	0.948	5.04	0.951	3.53	0.870	5.11	0.955	3.80	0.880	4.00	0.880
4.47	0.937	5.70	0.977	5.51	0.973	3.83	0.890	5.59	0.973	4.27	0.902	4.39	0.899
4.93	0.964	6.21	0.988	6.03	0.988	4.27	0.911	6.20	0.990	4.66	0.929	4.82	0.917
5.56	0.991	6.92	0.994	6.86	0.996	4.65	0.935	7.18	0.999	5.32	0.949	5.20	0.938
6.40	0.999	7.97	0.998	7.46	0.998	5.02	0.954	8.42	1.000	5.88	0.968	5.64	0.953
7.22	1.000	8.88	1.000	8.13	0.998	5.47	0.975			6.36	0.983	6.14	0.971
				8.79	0.999	6.10	0.993			7.11	0.995	6.71	0.986
						6.86	0.998			8.53	0.998	7.52	0.998
						7.73	1.000			10.21	0.999		

(e) Downstream of corner, 8° shock at corner

X = 19.0		X = 25.4		X = 38.1		X = 50.8		X = 76.2		X = 101.6		X = 127.0	
Y	u/U	Y	u/U	Y	u/U	Y	u/U	Y	u/U	Y	u/U	Y	u/U
0.0	0.0	0.0	0.0	0.0	0.0	0.0	0.0	0.0	0.0	0.0	0.0	0.0	0.0
0.09	0.233	0.09	0.282	0.09	0.377	0.09	0.422	0.09	0.480	0.09	0.490	0.09	0.501
0.51	0.307	0.86	0.395	0.47	0.460	0.20	0.488	0.18	0.540	0.20	0.557	0.27	0.580
1.06	0.385	1.55	0.486	1.37	0.546	0.62	0.546	0.41	0.601	0.37	0.610	0.45	0.628
1.59	0.487	2.25	0.592	2.04	0.619	1.40	0.607	0.81	0.641	0.76	0.658	0.88	0.677
2.02	0.566	2.59	0.650	2.53	0.683	2.06	0.664	1.52	0.686	1.36	0.700	1.75	0.730
2.43	0.651	2.96	0.705	2.92	0.732	2.46	0.707	2.38	0.743	2.01	0.739	2.70	0.774
2.77	0.706	3.26	0.745	3.27	0.768	2.90	0.752	3.09	0.793	2.75	0.780	3.28	0.806
3.11	0.749	3.49	0.778	3.55	0.804	3.27	0.788	3.58	0.830	3.25	0.811	3.87	0.834
3.48	0.795	3.81	0.813	3.89	0.841	3.68	0.832	4.15	0.868	3.81	0.843	4.54	0.867
3.78	0.829	4.11	0.640	4.28	0.872	4.08	0.864	4.45	0.891	4.22	0.868	5.19	0.904
4.21	0.865	4.53	0.881	4.59	0.899	4.41	0.891	4.85	0.916	4.68	0.896	5.67	0.924
4.52	0.895	4.96	0.920	4.91	0.927	4.80	0.921	5.32	0.944	5.30	0.931	6.08	0.945
4.91	0.929	5.29	0.943	5.29	0.950	5.15	0.943	5.75	0.967	5.80	0.956	6.55	0.963
5.36	0.962	5.60	0.965	5.59	0.969	5.46	0.961	6.33	0.985	6.53	0.981	7.30	0.984
5.66	0.981	5.95	0.984	5.98	0.986	5.93	0.981	7.42	0.998	7.57	0.996	8.03	0.994
6.42	0.999	6.48	0.993	6.99	1.000	6.96	0.997	8.76	1.000	8.79	0.999	8.88	0.998
7.51	1.000	7.14	0.999			8.03	0.998	9.91	1.000	10.51	1.000	9.73	1.000
		8.07	1.001			9.06	1.000					10.69	1.000

(f) Downstream of corner, 6° shock 20 mm upstream of corner

X = 19.0		X = 25.4		X = 38.1		X = 50.8		X = 76.2		X = 101.6		X = 127.0	
Y	u/U	Y	u/U	Y	u/U	Y	u/U	Y	u/U	Y	u/U	Y	u/U
0.0	0.0	0.0	0.0	0.0	0.0	0.0	0.0	0.0	0.0	0.0	0.0	0.0	0.0
0.09	0.524	0.09	0.517	0.09	0.531	0.09	0.537	0.09	0.547	0.09	0.540	0.09	0.535
0.09	0.555	0.16	0.565	0.17	0.590	0.22	0.562	0.35	0.649	0.37	0.648	0.24	0.615
0.34	0.604	0.32	0.613	0.38	0.645	0.25	0.610	0.58	0.681	0.60	0.679	0.44	0.668
0.56	0.639	0.56	0.654	0.65	0.684	0.34	0.657	0.80	0.712	0.85	0.711	0.75	0.706
1.15	0.686	1.14	0.696	1.14	0.719	0.67	0.694	1.10	0.737	1.26	0.738	1.23	0.740
1.72	0.727	1.72	0.737	1.69	0.754	1.21	0.736	1.70	0.770	1.60	0.755	1.79	0.771
2.26	0.768	2.36	0.778	2.31	0.785	2.01	0.776	2.28	0.799	2.07	0.782	2.49	0.802
2.68	0.802	2.78	0.811	2.82	0.824	2.69	0.816	2.73	0.821	2.60	0.808	3.08	0.828
3.08	0.833	3.22	0.843	3.28	0.853	3.27	0.846	3.27	0.849	3.25	0.837	3.69	0.858
3.45	0.861	3.61	0.866	3.64	0.877	3.73	0.874	3.74	0.872	3.86	0.867	4.33	0.881
3.79	0.885	3.92	0.888	3.99	0.899	4.23	0.901	4.23	0.897	4.45	0.893	4.86	0.904
4.14	0.906	4.26	0.911	4.34	0.918	4.73	0.924	4.67	0.917	5.16	0.922	5.40	0.926
4.48	0.929	4.57	0.930	4.73	0.938	5.14	0.943	5.17	0.939	5.86	0.951	5.93	0.946
4.94	0.951	4.88	0.947	5.08	0.954	5.58	0.962	6.01	0.972	6.58	0.077	6.57	0.967
5.30	0.969	5.72	0.979	5.34	0.967	6.09	0.980	7.01	0.993	7.32	0.982	7.28	0.983
5.66	0.961	6.35	0.993	5.68	0.980	7.01	0.993	8.15	1.000	8.13	0.998	8.06	0.994
6.38	0.994	7.19	0.999	6.15	0.991	8.42	0.997	9.00	1.001	8.92	1.000	9.16	0.998
7.50	0.999	8.22	0.999	6.60	0.997	9.50	0.998					10.40	1.000
8.62	1.000	9.22	1.000	7.51	0.999	10.68	0.999						
				8.60	1.000								

Table II (concluded)

(g) Downstream of corner, 6° shock 20 mm downstream of corner

X = 31.8		X = 38.1		X = 50.8		X = 63.5		X = 76.2		X = 101.6		X = 127.0	
Y	u/U	Y	u/U	Y	u/U	Y	u/U	Y	u/U	Y	u/U	Y	u/U
0.0	0.0	0.0	0.0	0.0	0.0	0.0	0.0	0.0	0.0	0.0	0.0	0.0	0.0
0.09	0.244	0.09	0.305	0.09	0.390	0.09	0.477	0.09	0.486	0.09	0.500	0.09	0.532
0.71	0.422	0.69	0.454	0.51	0.483	0.44	0.552	0.24	0.558	0.21	0.579	0.27	0.602
1.19	0.558	1.29	0.551	1.16	0.562	1.25	0.627	0.66	0.616	0.41	0.633	0.69	0.672
1.59	0.655	1.67	0.629	1.56	0.626	1.89	0.685	1.38	0.674	0.98	0.684	1.38	0.724
1.95	0.711	2.11	0.700	2.08	0.692	2.45	0.747	2.06	0.725	1.56	0.722	1.96	0.759
2.37	0.755	2.54	0.756	2.51	0.746	2.96	0.791	2.55	0.766	2.17	0.762	2.80	0.804
2.78	0.795	3.00	0.803	2.97	0.793	3.40	0.831	3.08	0.812	2.85	0.805	3.40	0.841
3.21	0.832	3.55	0.846	3.37	0.827	3.90	0.866	3.57	0.848	3.43	0.841	4.14	0.878
3.66	0.865	4.00	0.883	3.74	0.858	4.31	0.895	4.03	0.880	3.92	0.871	4.66	0.906
4.01	0.890	4.51	0.919	4.19	0.887	4.81	0.925	4.51	0.910	4.35	0.898	5.18	0.934
4.40	0.912	4.89	0.945	4.66	0.920	5.25	0.950	4.93	0.935	4.88	0.924	5.69	0.957
4.76	0.936	5.32	0.971	5.08	0.948	5.74	0.973	5.44	0.960	5.35	0.948	6.33	0.979
5.21	0.960	5.87	0.992	5.54	0.974	6.45	0.992	5.96	0.981	5.95	0.973	7.23	0.997
5.71	0.978	6.40	0.998	6.15	0.993	7.48	0.998	6.93	0.996	6.73	0.990	8.31	1.001
6.38	0.991	6.82	1.000	7.22	0.998	8.81	0.999	8.16	0.999	8.01	0.997		
7.09	1.000	7.65	1.000	8.27	1.000	10.53	1.000	9.60	1.000	9.46	0.998		
										11.11	1.000		

Symbols

c_f local skin-friction coefficient, $= \tau_w/(0.5\,\rho_1 U^2)$

H shape factor, $= \delta^*/\Theta$

M Mach number

p static pressure

p_o settling chamber stagnation pressure

p^+ $\dfrac{\nu_w}{\rho_w u_\tau^3}\dfrac{dp}{dx}$

p^* $\dfrac{\delta^*}{\tau_w}\dfrac{dp}{dx}$, Clauser's equilibrium parameter

R_Θ Reynolds number, $= U\Theta/\nu_1$

T static temperature

u streamwise mean velocity

U free stream mean velocity

u^+ u_i/u_τ

u_τ friction velocity, $= (\tau_w/\rho_w)^{\frac{1}{2}}$

x streamwise distance measured from expansion corner

x_s nominal shock impingement position

y distance along normal of wall

y^+ yu_τ/ν_w

Greek symbols

α angle of flow deflection by incident shock

δ boundary-layer thickness at $u/U = 0.995$

δ^* displacement thickness, equation (A.1)

Θ momentum thickness, equation (A.1)

ν kinematic viscosity

ρ mean density

τ total shear stress i.e. laminar plus Reynolds shear stresses

Subscripts

i Van Driest's transformed incompressible condition

k kinematic condition

1 at free stream condition

w at the wall

References

1 Y.T. Chew — The turbulent boundary layer at an expansion corner with shock waves. Ph.D. Dissertation, Cambridge University, 1976

2 Y.T. Chew — Features of the flow at an expansion corner with shock disturbances. To be published

3 L.O.F. Jeromin — An experimental investigation of the compressible turbulent boundary layer with air injection. ARC R & M 3526, 1966

4 L.C. Squire — Further experimental investigations of compressible turbulent boundary layers with air injection. ARC R & M 3627, 1970

5 D.I.A. Dunbar, L.C. Squire — Experiments in turbulent boundary layers with foreign gas injection. ARC R & M 3696, 1972

6 G.D. Thomas — Compressible turbulent boundary layers with combined air injection and pressure gradient. ARC R & M 3779, 1976

7 P.G. Marriott — Compressible turbulent boundary layers with discontinuous air transpiration: an experimental and theoretical investigation. ARC R & M 3780, 1977

8 J.M. Allen — Impact probe displacement in a supersonic turbulent boundary layer. NASA TN D-6759, 1972

9 K.G. Winter, L. Gaudet — Turbulent boundary-layer studies at high Reynolds numbers at Mach numbers between 0.2 and 2.8. ARC R & M 3712, 1970

10 E.J. Hopkins, E.R. Keener — Study of surface pitots for measuring turbulent skin-friction at supersonic Mach numbers. NASA TN D-3478, 1966

11 J.M. Allen — Evaluation of compressible-flow Preston tube calibrations. NASA TN D-7190, 1973

12 F.K. Owen, C.C. Horstman, M.I. Kussoy — Mean and fluctuating flow measurements of a fully-developed, non-adiabatic hypersonic boundary layer. J. Fluid Mechanics, Vol. 70, pp 393-413, 1975

13 R. Narasimha, A. Prabhu — Equilibrium and relaxation in turbulent wakes. J. Fluid Mechanics, Vol. 54, pp 1-17, 1972

14 A.A. Townsend — The Structure of Turbulent Shear Flow. CUP 1st Edn. 1956

15 Y.T. Chew — Two-parameter skin-friction formula for adiabatic compressible flow. AIAA Jour. Vol. 16, p 186, 1978

16 V.C. Patel — A unified view of the law of the wall using mixing length theory. Aero. Quart. Vol. 24, pp 55-70, 1973

17 R.A.McD.Galbraith, M.R. Head — Eddy viscosity and mixing length from measured boundary layer developments. Aero. Quart. Vol. 26, pp 133-154, 1975

18 D.E. Coles, E.A. Hirst — Computation of turbulent boundary layers. AFOSR-IFP Stanford Conf. Vol. 2, 1968

19 J.E. Lewis, R.L. Gran, T. Kubota — An experiment on the adiabatic compressible turbulent boundary layer in adverse and favourable pressure gradients. J. Fluid Mechanics,Vol. 51, pp 657-672, 1972

20 F.M. White — Viscous Fluid Flow. McGraw-Hill, 1974

21 L.C. Squire — A law of the wall for compressible turbulent boundary layers with air injection. J. Fluid Mechanics,Vol. 37, pp 449-456, 1969

22 G. Maise, H. McDonald — Mixing length and kinematic viscosity in a compressible boundary layer. AIAA Jour. Vol. 6, pp 73-80, 1968

23 D. Coles — The law of the wake in the turbulent boundary layer. J. Fluid Mechanics,Vol. 1, pp 191-225, 1956

24 T. Cebeci, A.M.O. Smith — Analysis of Turbulent Boundary Layers. Academic Press. 1974

25 V.K. Verma — A method for the calculation of two-dimensional and axisymmetric boundary layers. CUED/A-Aero/TR3, Cambridge University Engineering Department, 1973

26 P. Bradshaw, D.H. Ferriss, N.P. Atwell — Calculation of boundary layer development using the turbulence energy equation. J. Fluid Mechanics,Vol. 28, pp 593-616, 1967

27 M.J. Smith — Interaction of a shock wave with a boundary layer disturbed by injection. Ph.D. Dissertation, Cambridge University, 1976

28 P. Bradshaw — The effect of mean compression or dilation on the turbulent structure of supersonic boundary layers. J. Fluid Mechanics,Vol. 63, pp 449-464, 1974

29 L.C. Squire, V.K. Verma — The calculation of compressible turbulent boundary layers with injection. ARC C.P. 1265, 1973

30 G.D. Kuhn, J.N. Nielson — Prediction of turbulent separated flow at subsonic and transonic speeds including unsteady effects. AGARD-CP-168 Paper 26, 1975

31 W.C. Rose, D.A. Johnson
Turbulence in a shock wave boundary layer interaction.
AIAA Jour. Vol. 13, pp 884-887, 1975

32 J.D. Murphy, L.L. Presley, W.C. Rose
On the calculation of supersonic separating and reattaching flows.
AGARD-CP-168 Paper 22, 1975

33 J.S. Shang, W.L. Hankey
Supersonic turbulent separated flows utilizing the Navier Stokes equation.
AGARD-CP-168 Paper 23, 1975

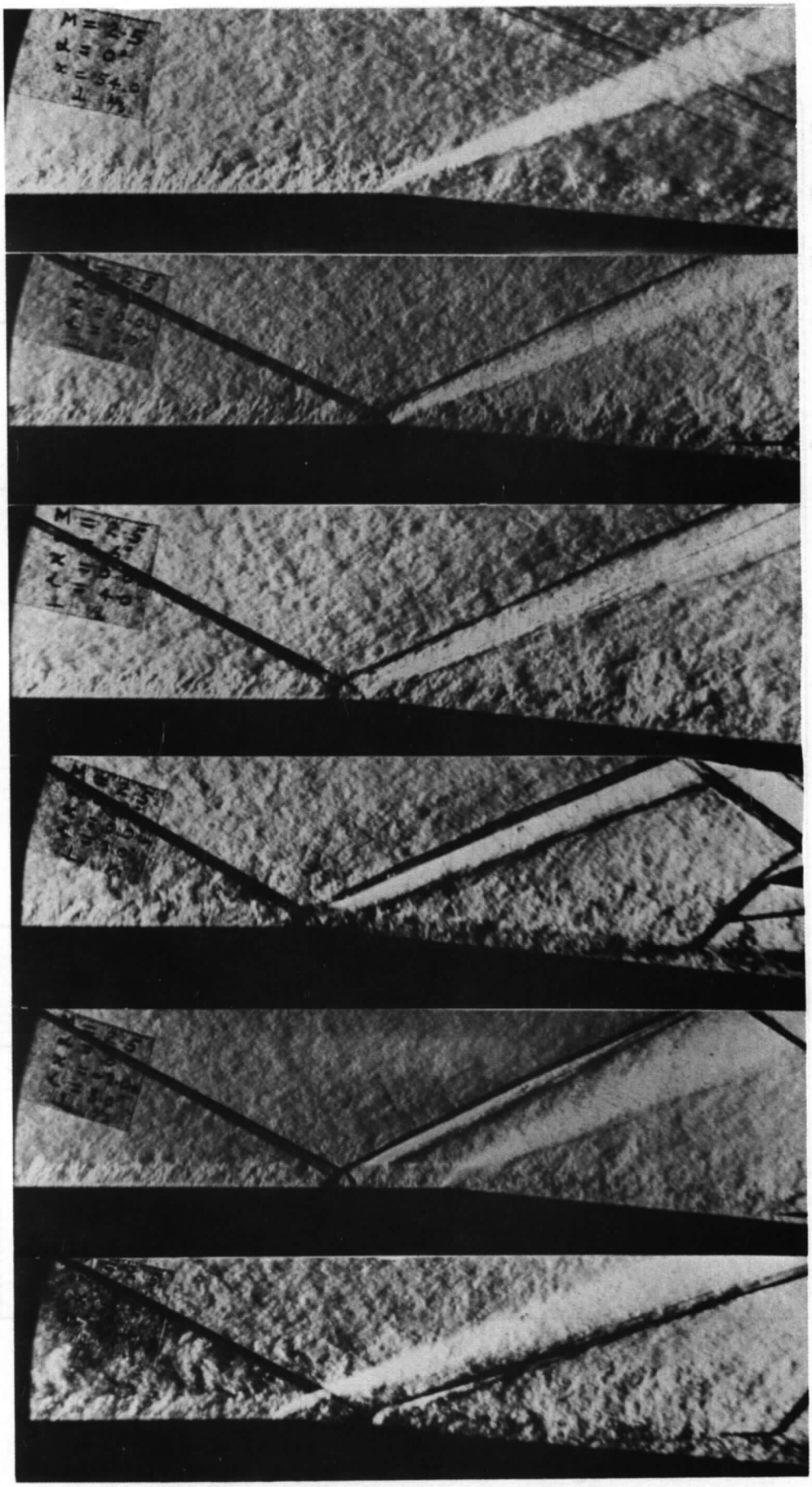

Cases (a) and (b)
No shock

Case (c)
4° shock at
corner

Case (d)
6° shock at
corner

Case (e)
8° shock at
corner

Case (f)
6° shock 20 mm
upstream of
corner

Case (g)
6° shock 20 mm
downstream of
corner

Fig 1 Schlieren photographs of the test conditions

Fig 2

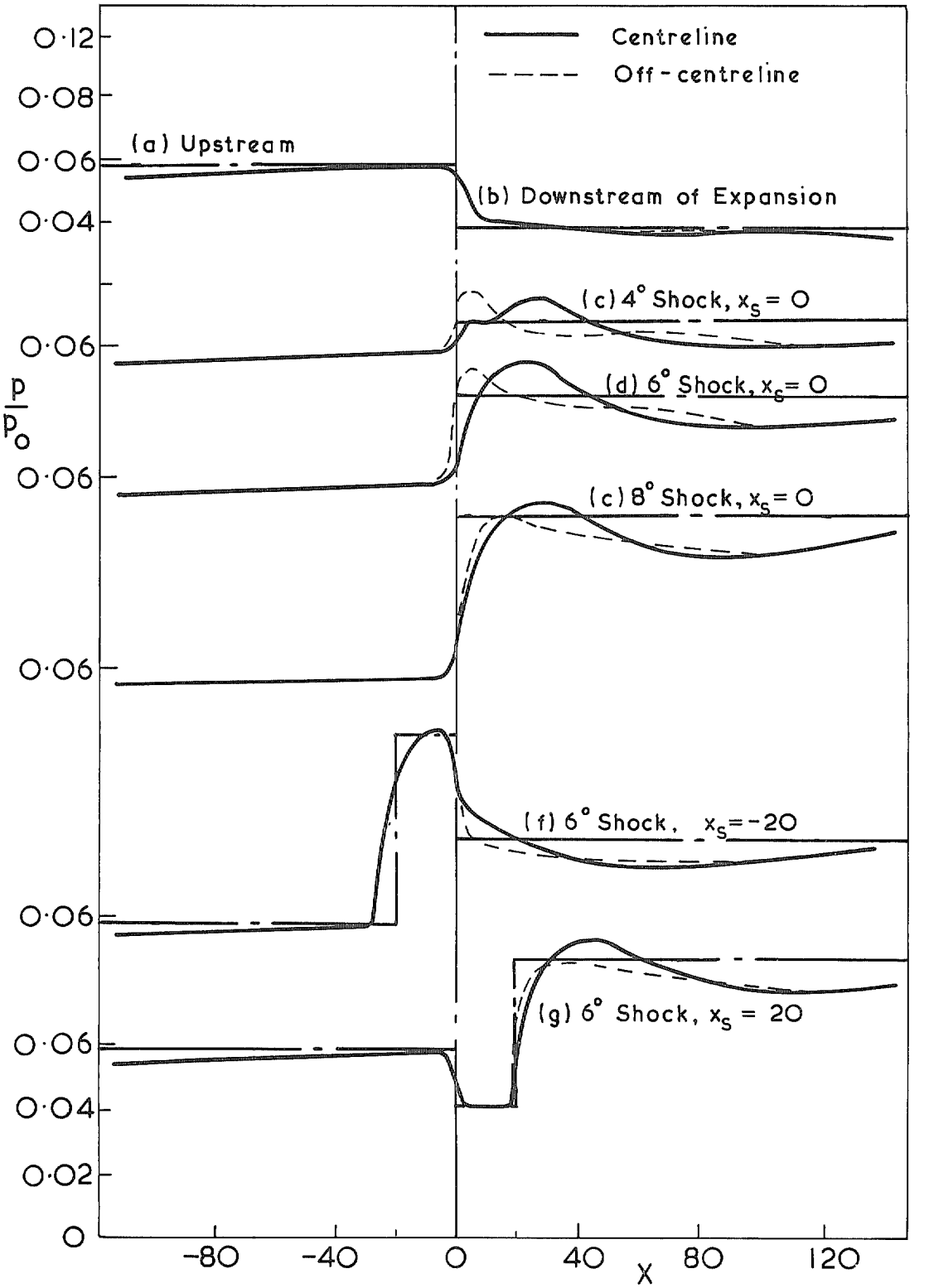

Fig 2 Pressure distributions

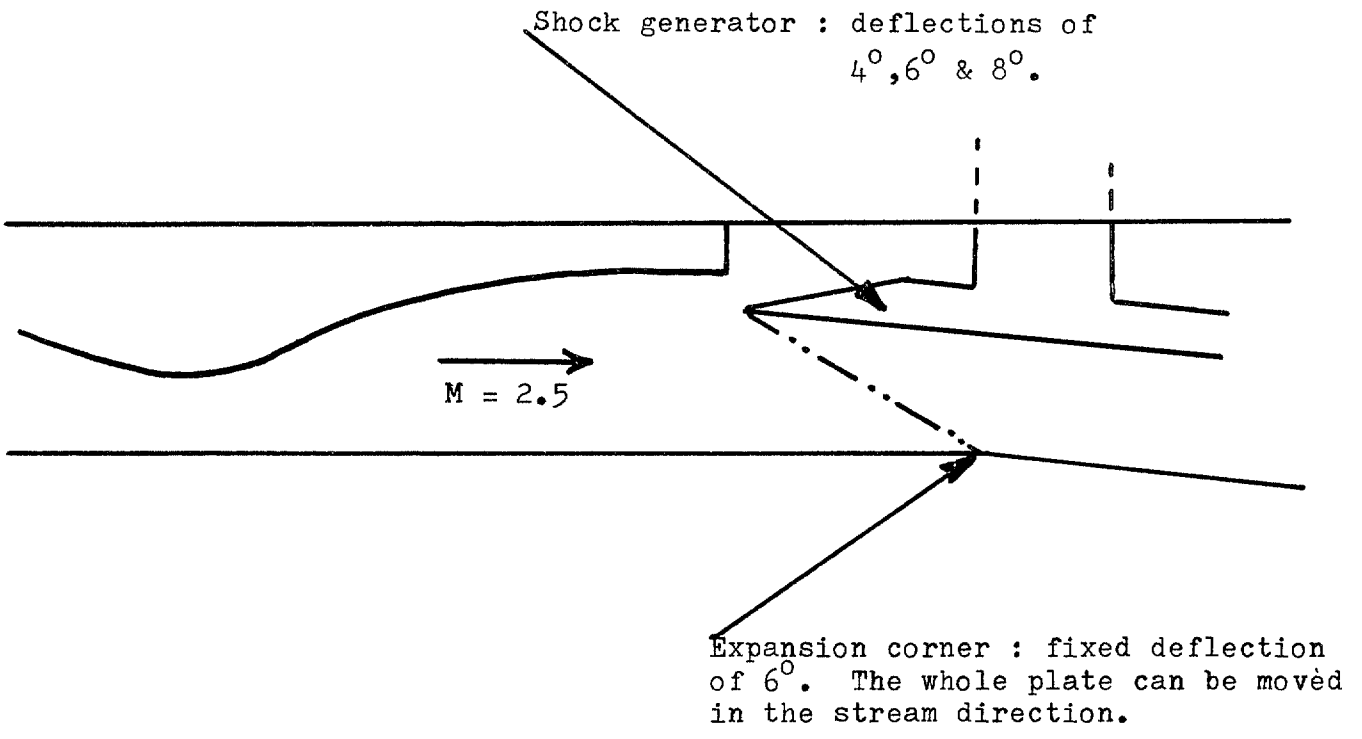

The expansion-corner plate contains 186 pressure holes in three rows in the stream direction. The pressure holes at the corner are drilled along the bisector of the angle.

Distance from throat to corner :	No shock	540mm
	4° shock at corner	543mm
	6° shock at corner	535mm
	8° shock at corner	523mm
Width of test section		114mm
Height of test section at end of nozzle		82mm

Fig 3 Details and sketch of test section

Fig 4a&b

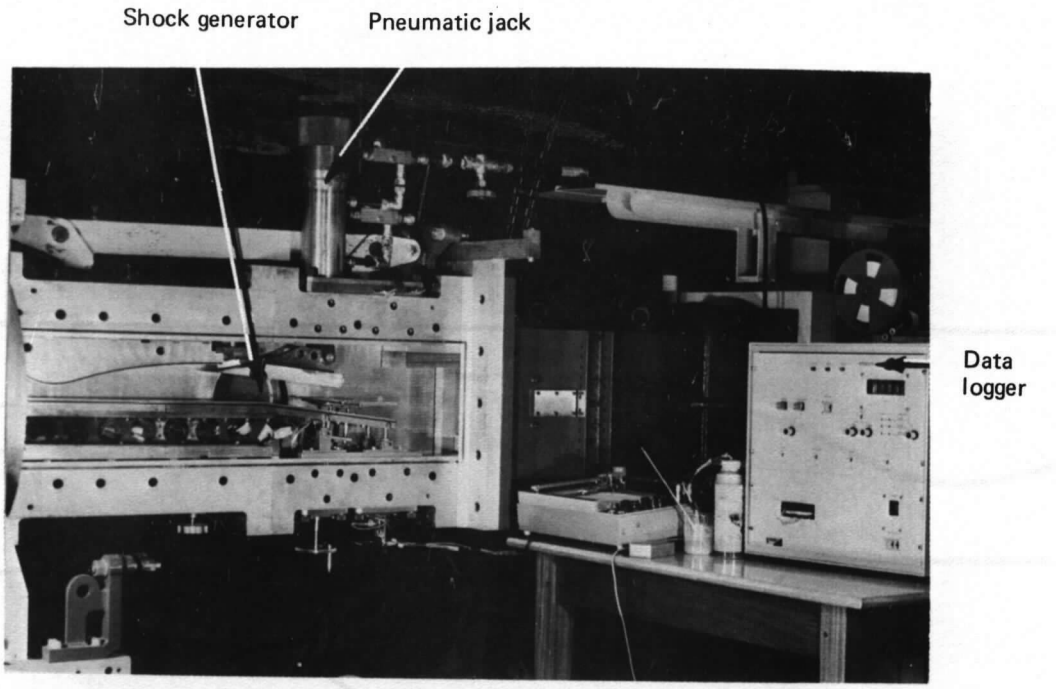

a Traverse gear arranged to measure boundary layer profiles downstream of the expansion corner

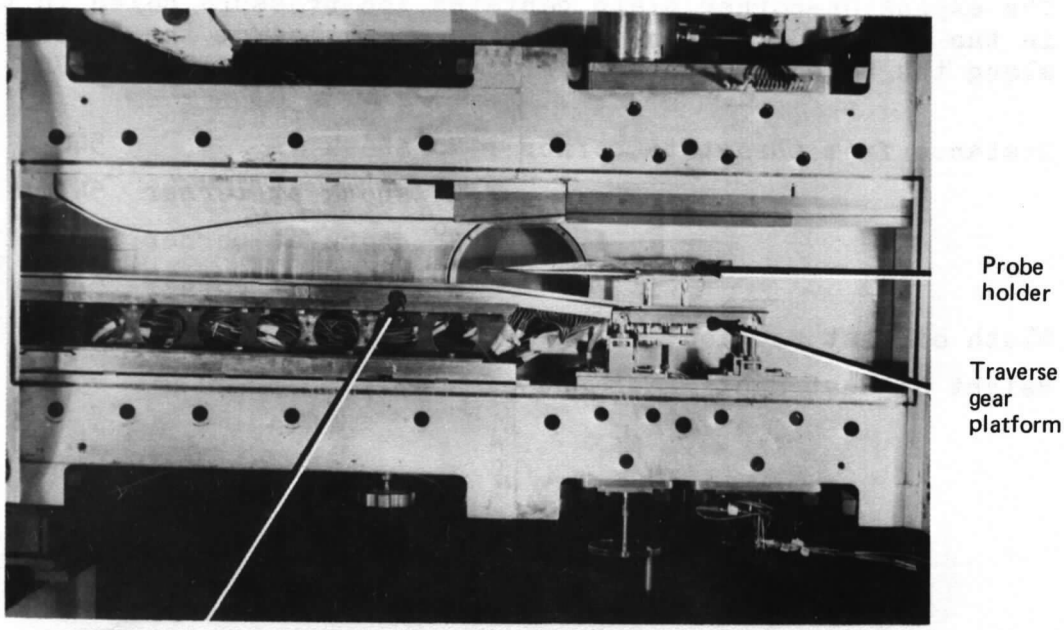

b Traverse gear arranged to measure boundary layer profiles upstream of the expansion corner

Fig 4a&b Photographs of the test section

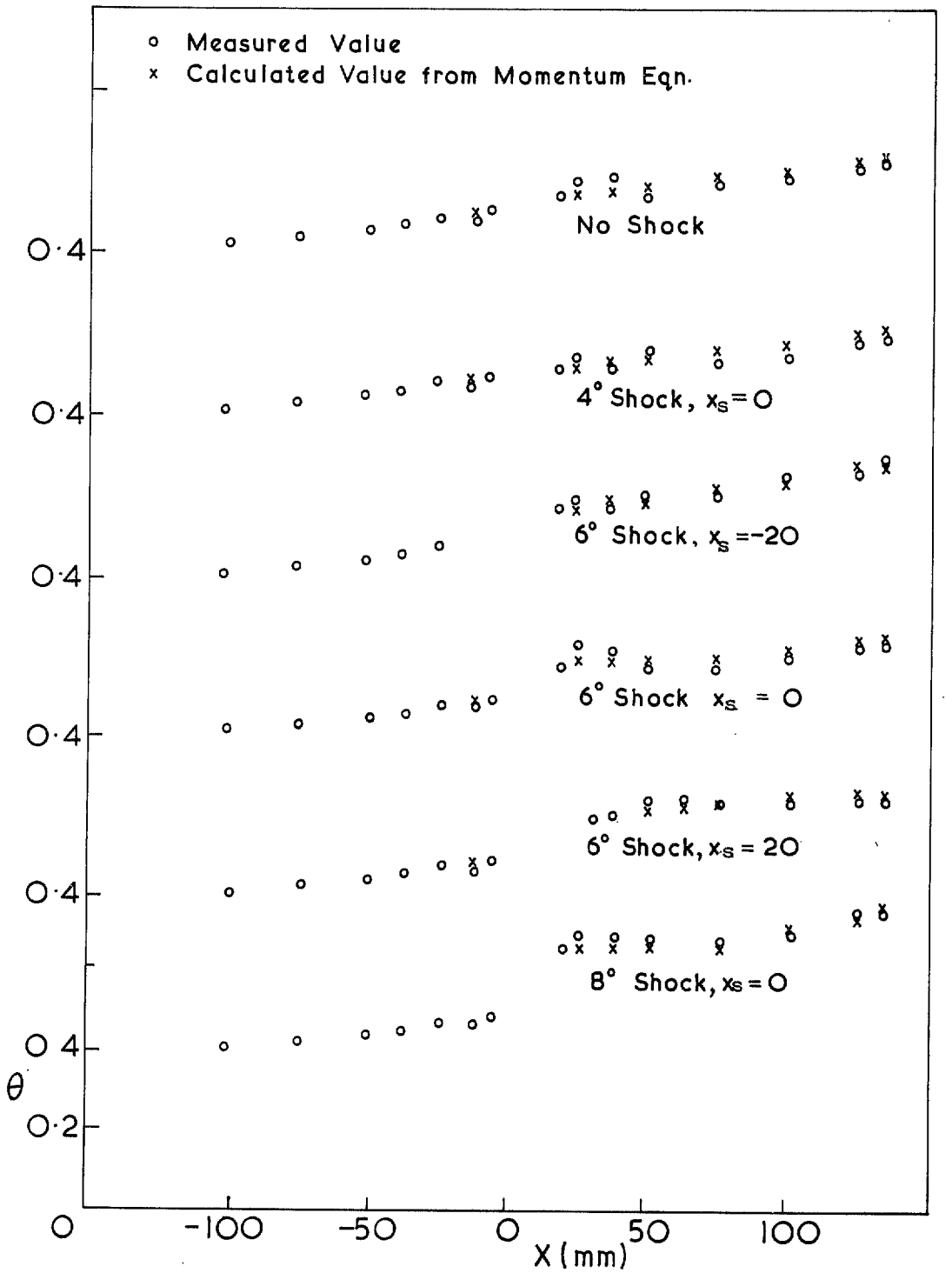

Fig 5a Variation of θ with X

Fig 5b

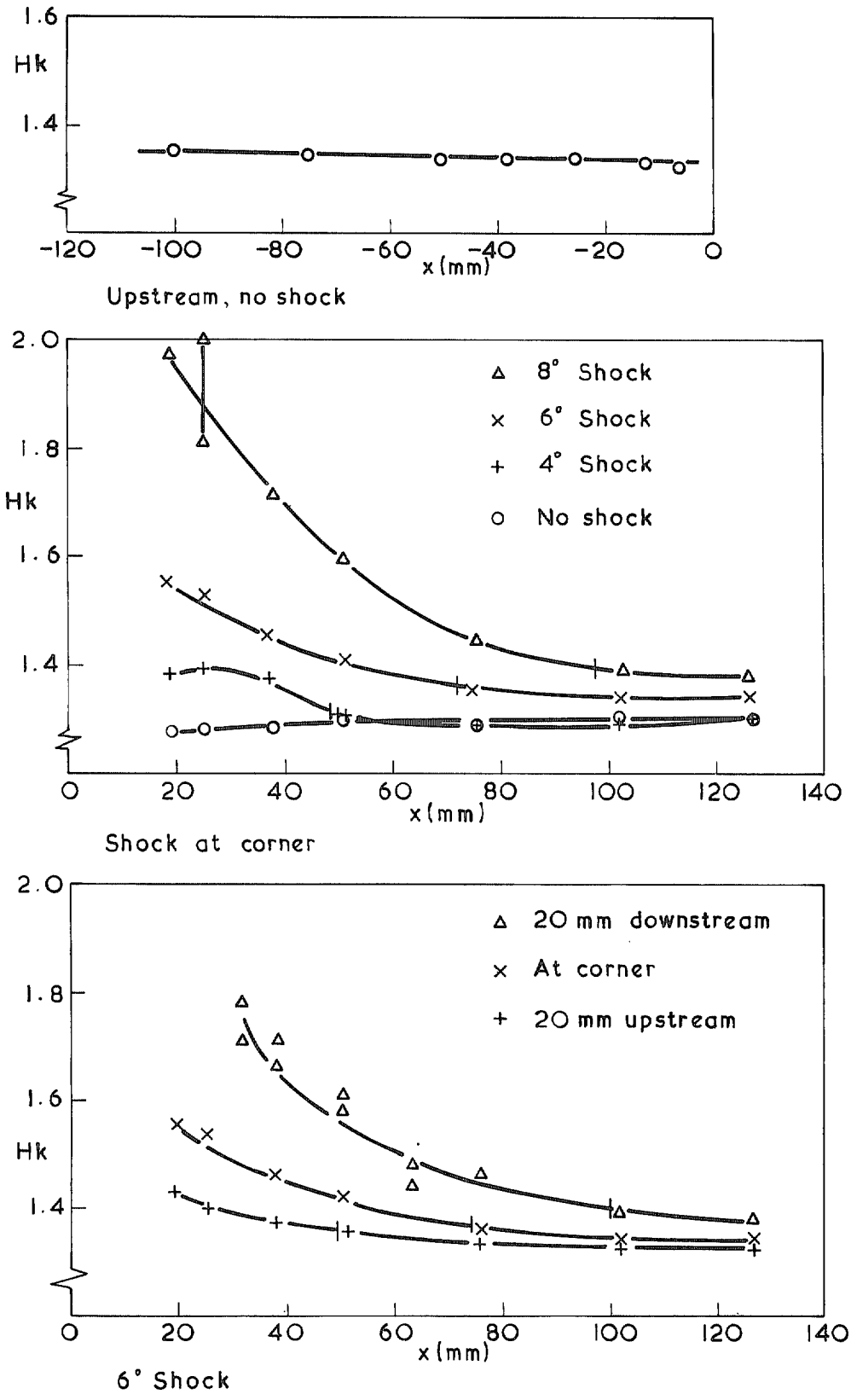

Fig 5b Variation of H_k with distance

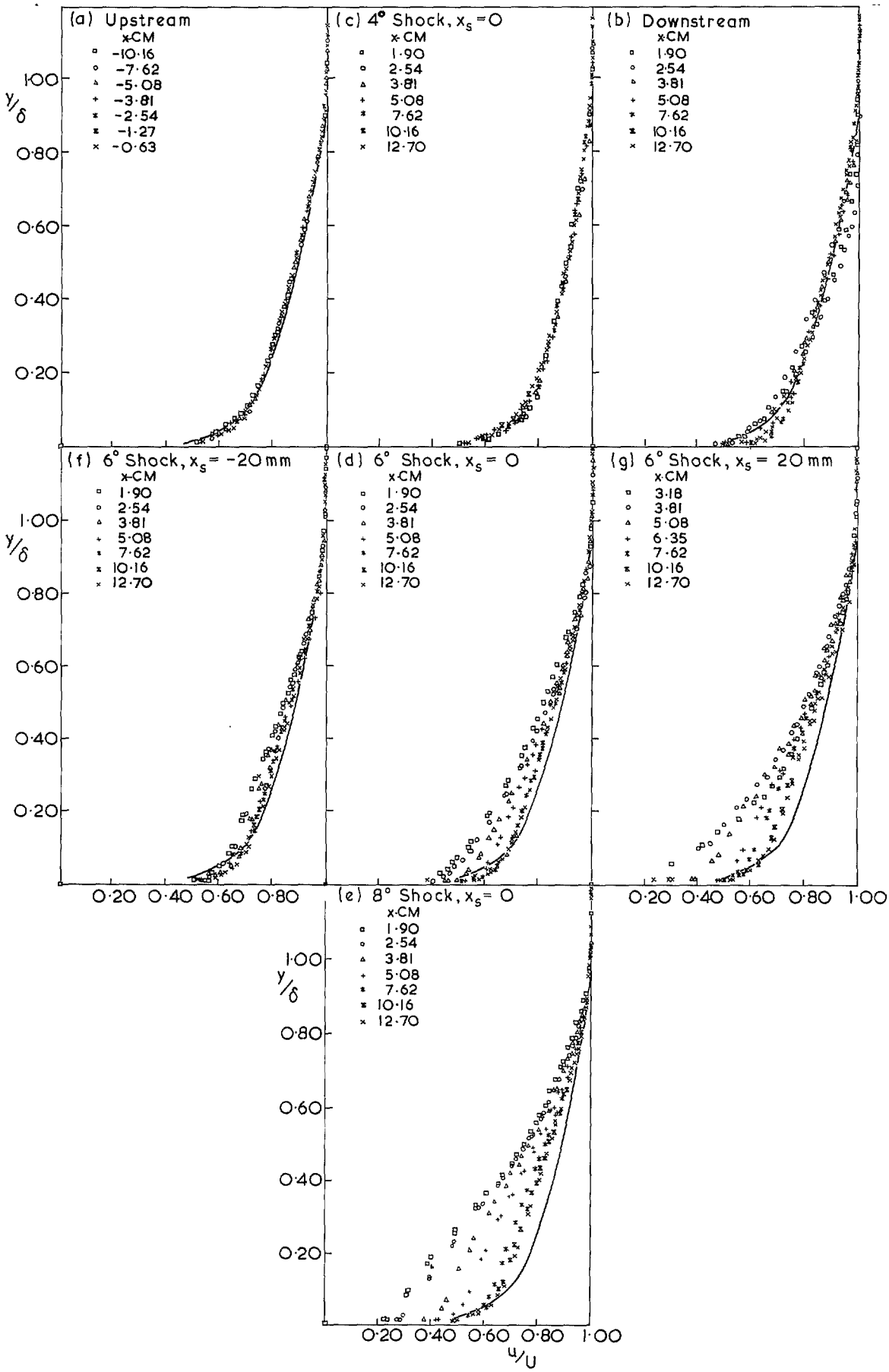

Fig 6a-g Velocity profiles

Fig 7a-g

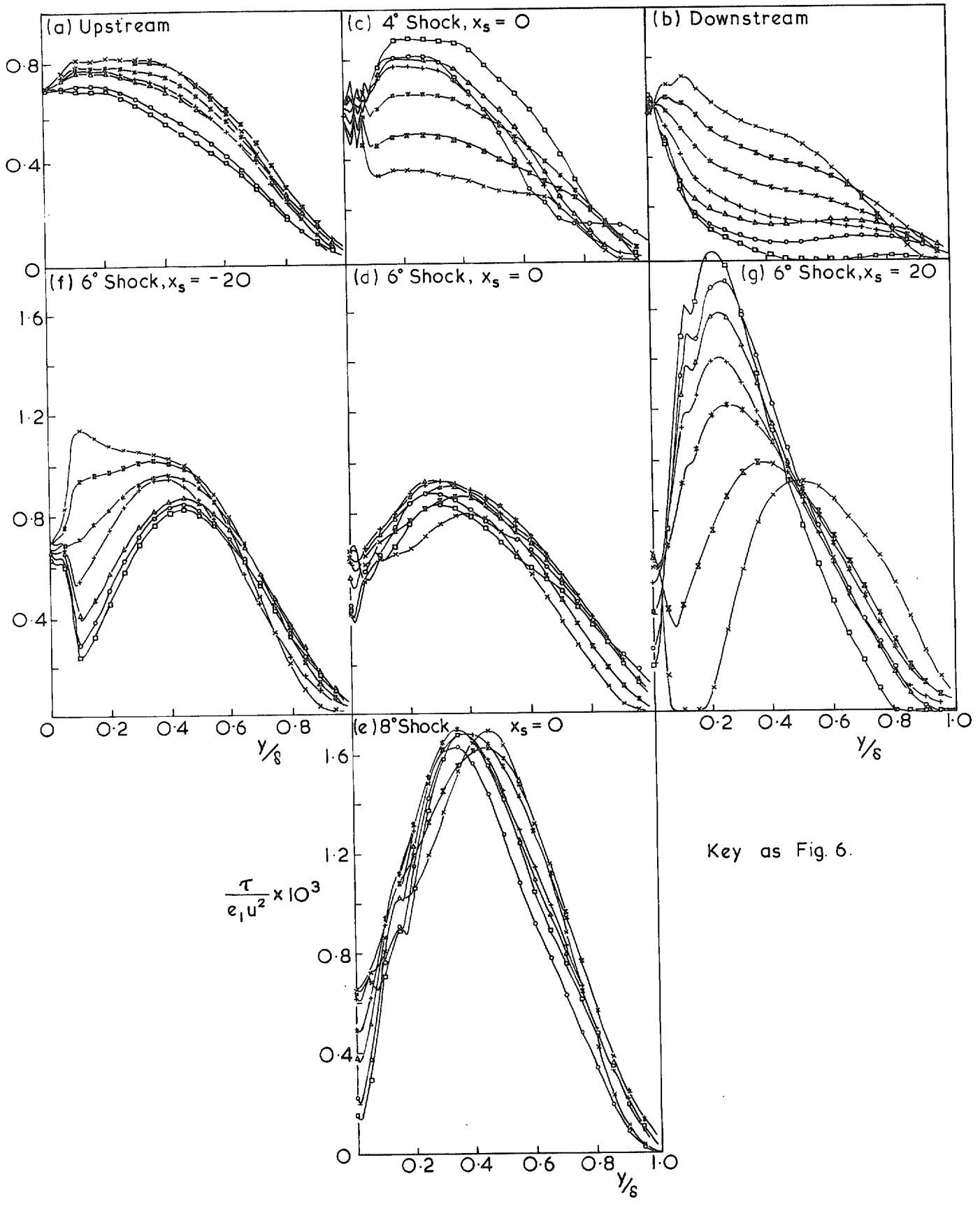

Fig 7a-g Shear-stress profiles

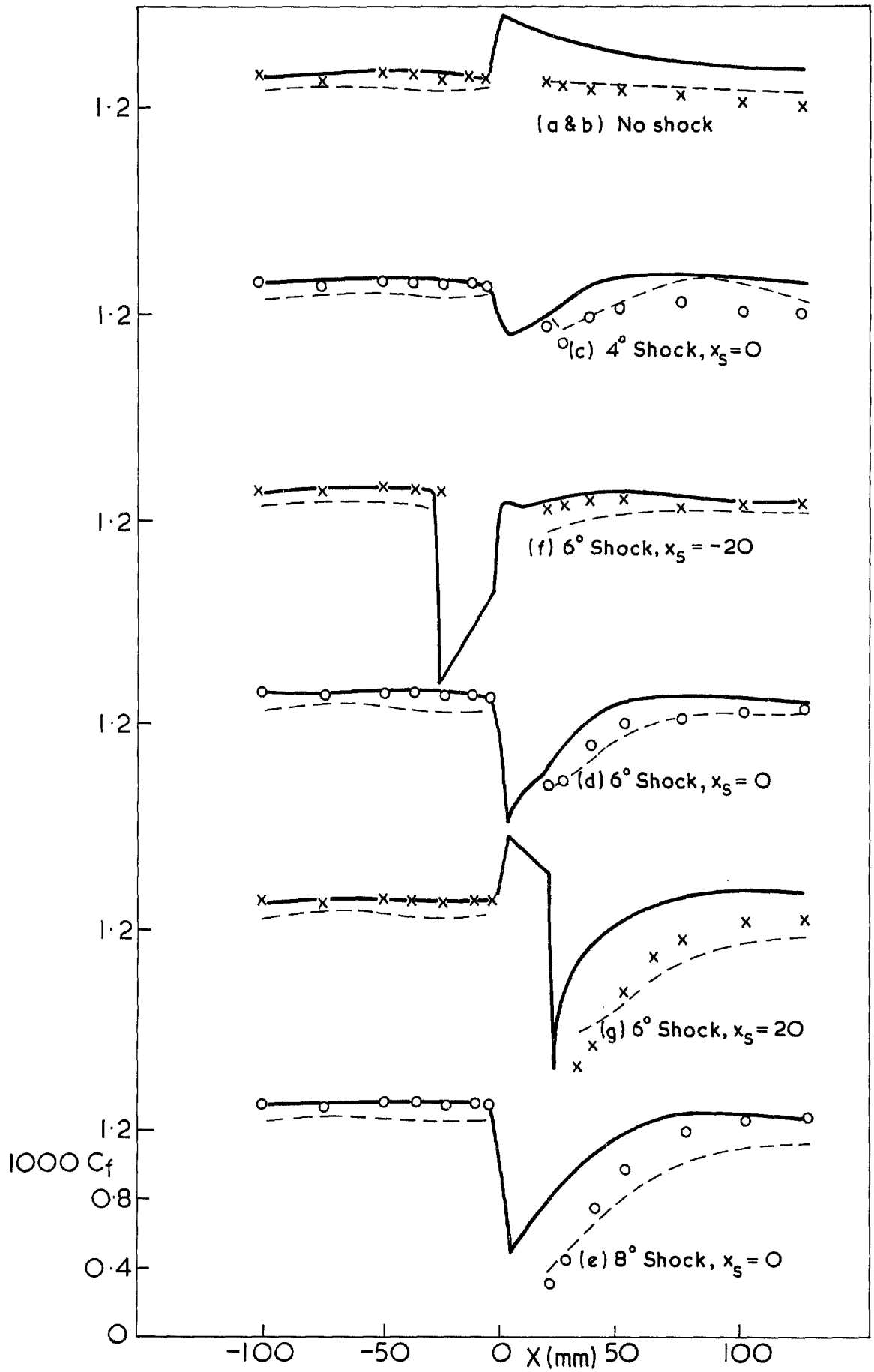

Fig 8 Measured and calculated skin-friction

Fig 9a-d

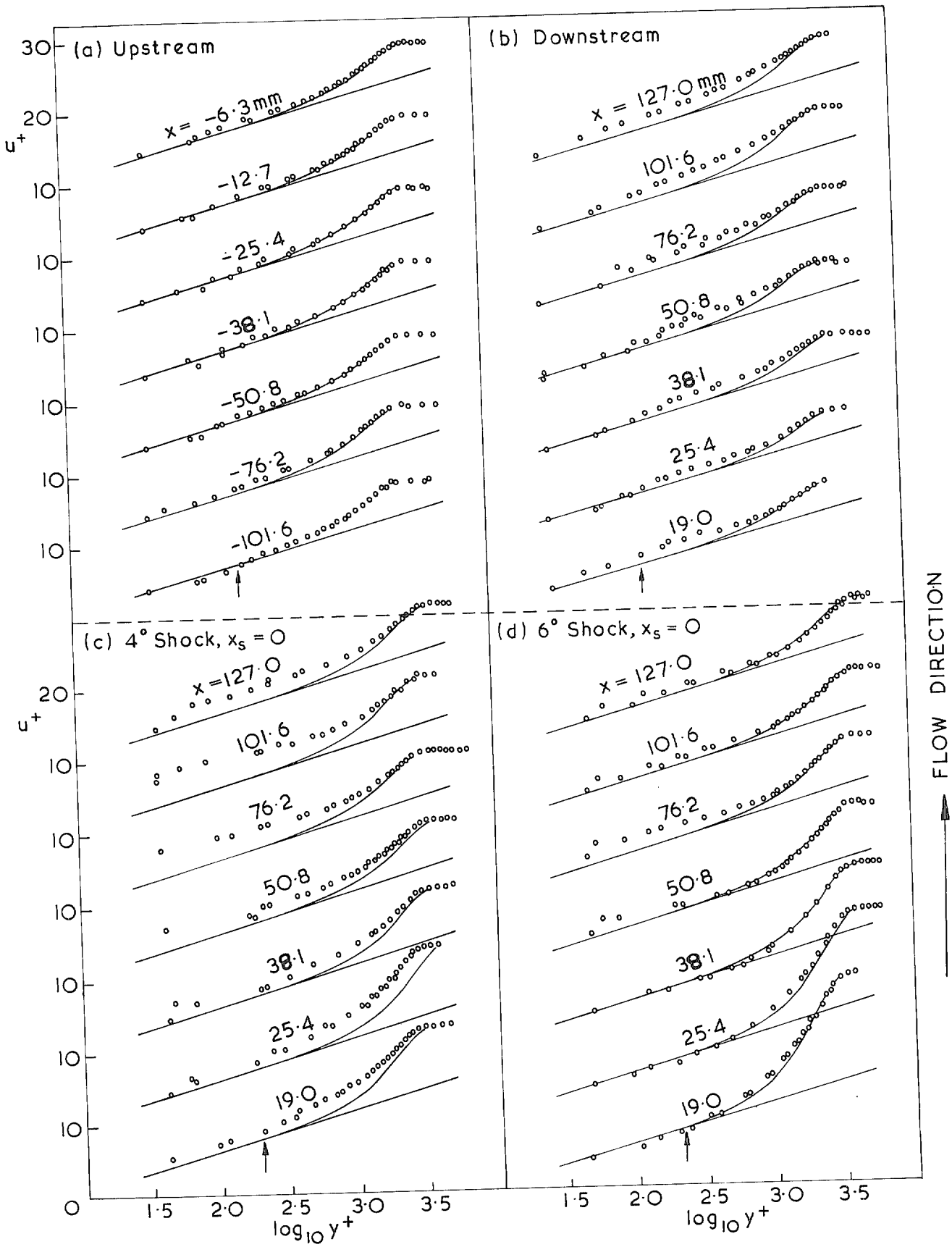

Fig 9a-d Law of the wall

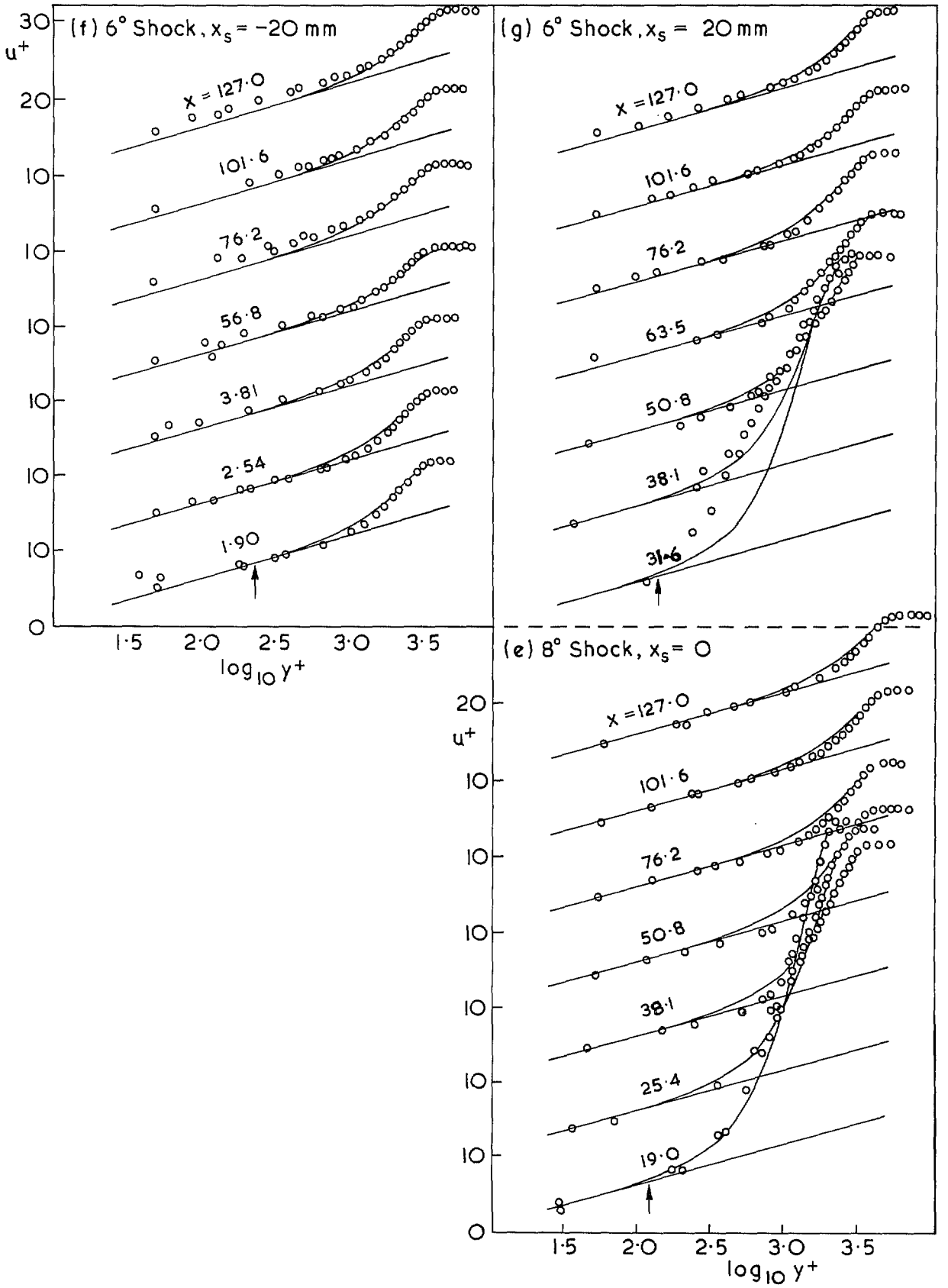

Fig 9e-g Law of the wall

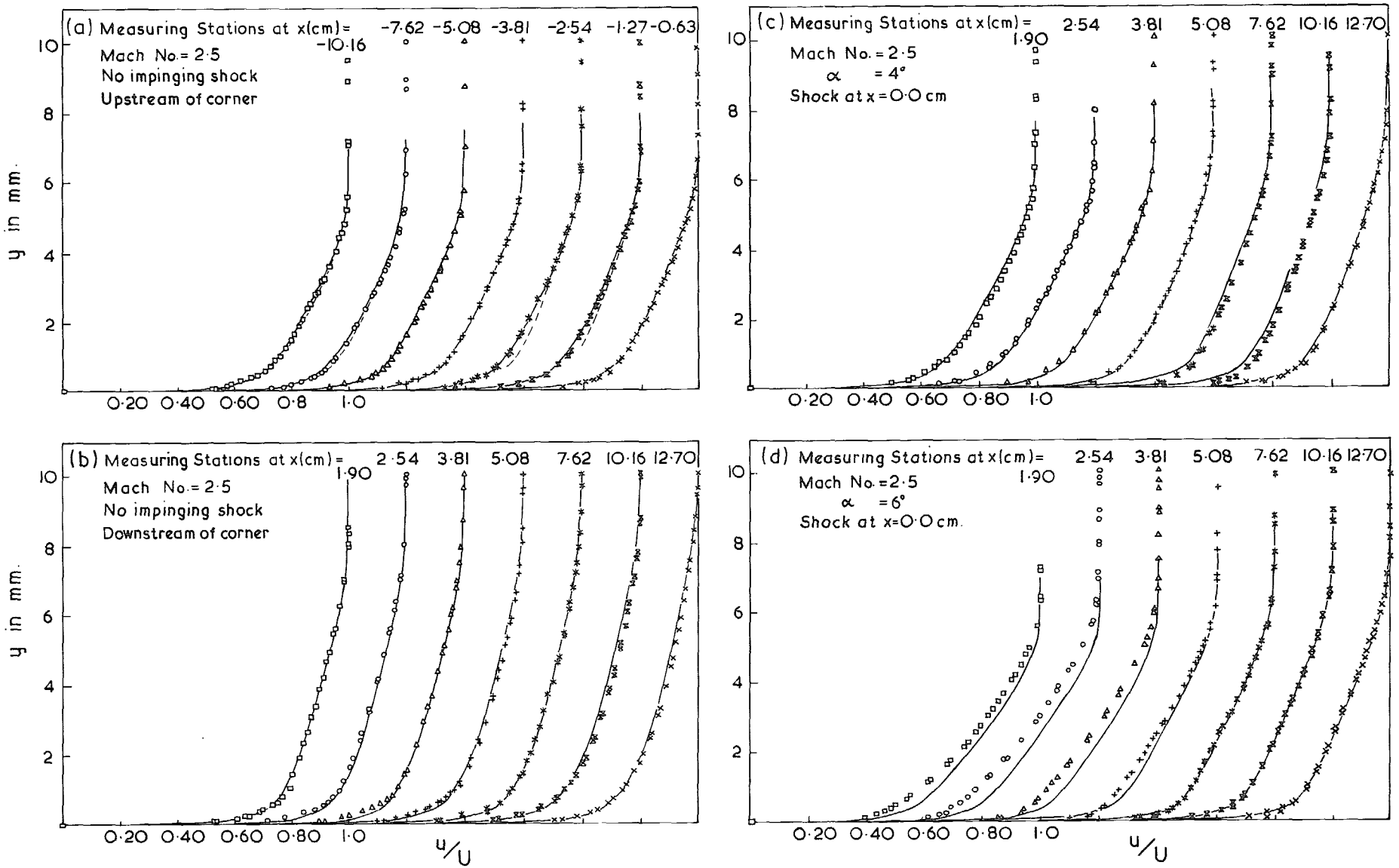

Fig 10a-d Velocity developments — comparison with predictions

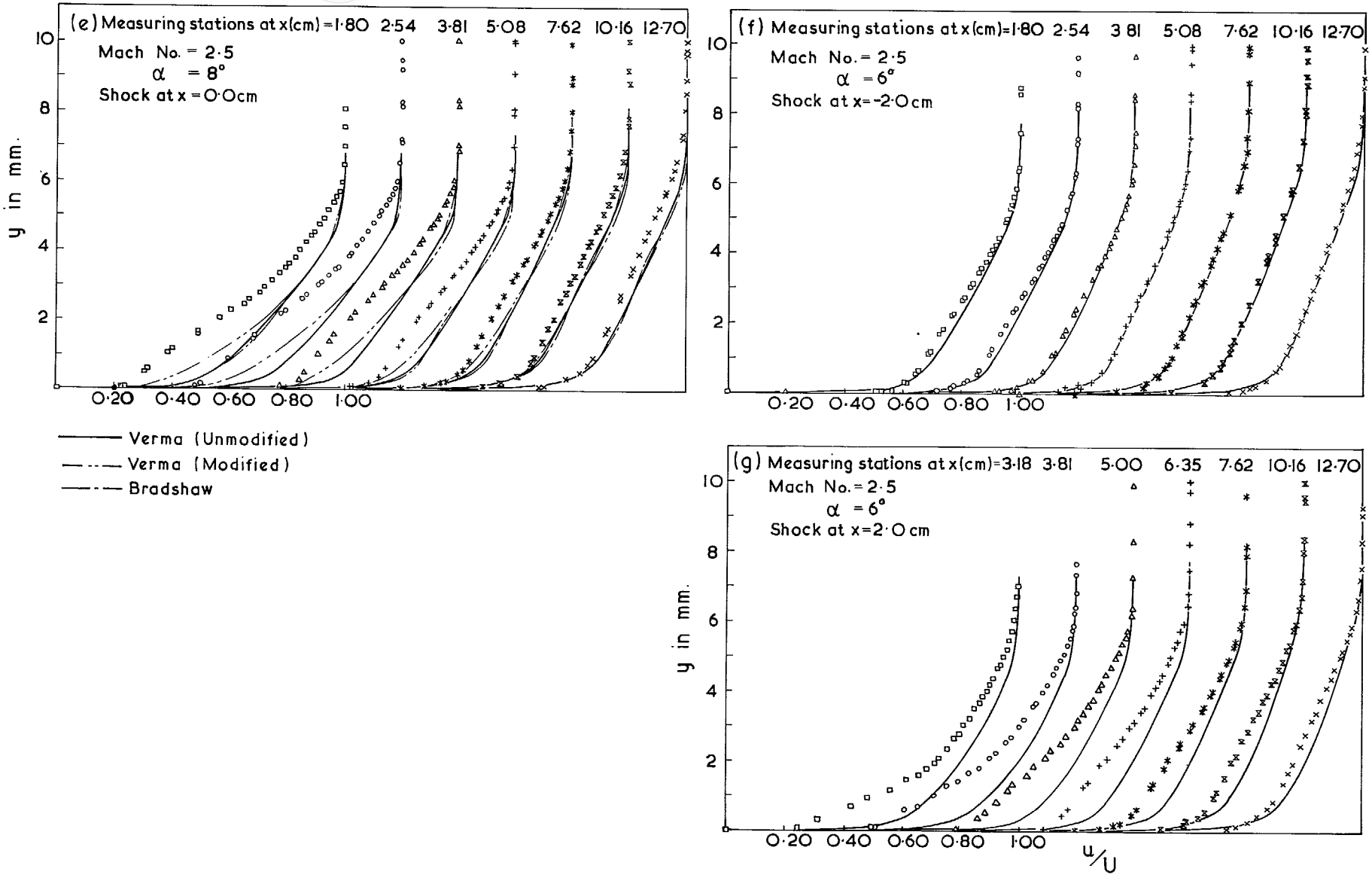

Fig 10e-g Velocity developments — comparison with predictions

Fig 10e-g

Fig 11

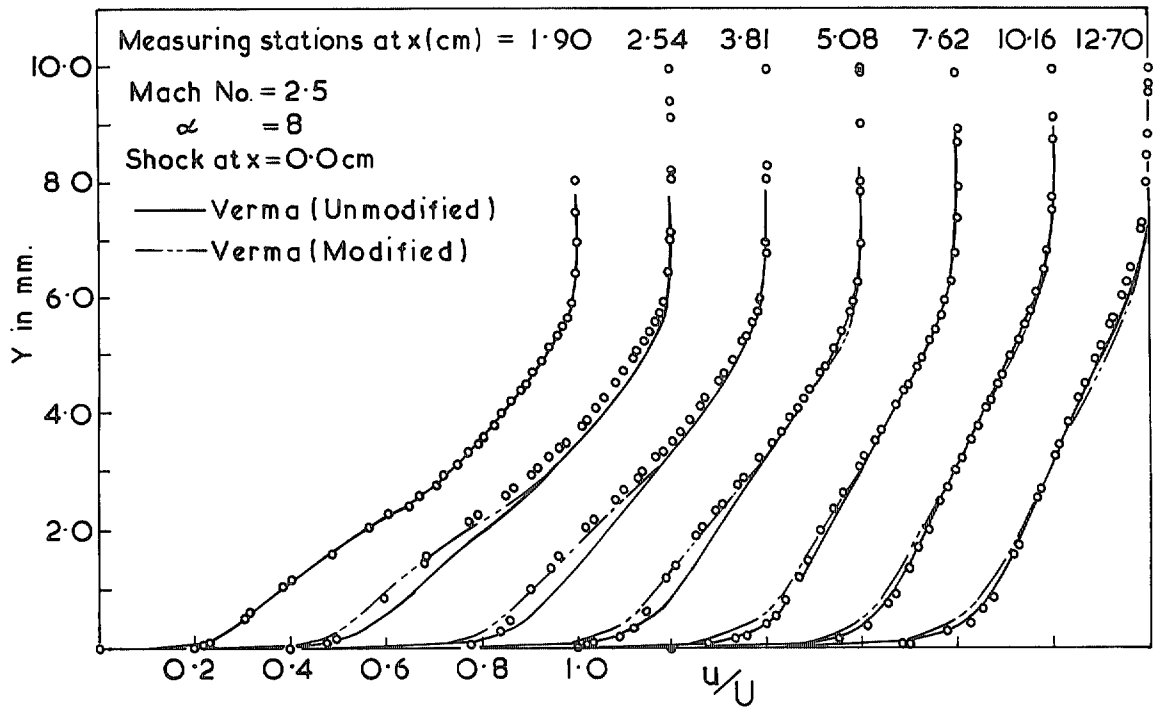

Fig 11 Comparison with modified eddy-viscosity model

Printed in England for Her Majesty's Stationery Office by the Royal Aircraft Establishment, Farnborough. Dd. 596060 K4 10/79.

First published 1979

HER MAJESTY'S STATIONERY OFFICE

Government Bookshops
49 High Holborn, London WC1V 6HB
13a Castle Street, Edinburgh EH2 3AR
41 The Hayes, Cardiff CF1 1JW
Brazennose Street, Manchester M60 8AS
Southey House, Wine Street, Bristol BS1 2BQ
258 Broad Street, Birmingham B1 2HE
80 Chichester Street, Belfast BT1 4JY

Government Publications are also available through booksellers

R & M No. 3839
ISBN 0 11 471172 0